N72-12940

NASA CR-111965

LEADING EDGE COOLING BY UPSTREAM INJECTION*

CASE FILE COPY

by

Renzo Piva†

*The work reported herein was supported by the National Aeronautics and Space Administration, under Grant No. NGR-33-016-131

†Visiting Adjunct Professor, New York University Aerospace Laboratory (Assistant Professor of Aerodynamics, University of Rome, Italy)

FOREWORD

This report was prepared under the National Aeronautic and Space Administration, under Grant No. NGR-33-016-131. This grant supports research involving the problem of engine airplane integration and cooling. The author wishes to thank Dr. Antonio Ferri for suggesting this research and for his guidance during the progress of the investigation. Mr. Richard Poch and Carlos De Jesus are also cited for their helpful collaboration.

TABLE OF CONTENTS

	PAGE
ABSTRACT	ii
NOMENCLATURE	iii
LIST OF FIGURES	v
INTRODUCTION	1
DESCRIPTION OF THE PHYSICAL PHENOMENA - GOVERNING PARAMETERS	2
APPROACH TO THE STUDY	6
EXPERIMENTAL INVESTIGATION	6
a) Experimental Equipment	6
b) Model	7
c) Measurements	8
d) Test Results	10
e) Correlation of Data	12
THEORETICAL ANALYSIS	13
a) Basic Equations and Hypothesis	14
b) Similar Solution	15
c) Non-similar Solution	17
d) Locally Similar Solution	20
COMPUTATION OF THE TEMPERATURE FIELD INSIDE THE BODY	21
APPLICATIONS AND COMPARISONS	22
CONCLUDING REMARKS	23
REFERENCES	25
APPENDIX I	69
APPENDIX II	71

ABSTRACT

A leading edge cooling system by upstream injection along the surface has been investigated. The purpose of this system is to keep the leading edge below a desired temperature without excessively increasing the radius of the tip and consequently the total pressure losses.

An experimental investigation has been conducted to find the optimum conditions for the cooling from the point of view of upstream jet penetration and minimum shock losses. A theoretical analysis was performed to study the flow field in the mixing region between the two counterflowing streams and the results obtained compare favorably with the experimental results.

NOMENCLATURE

D	drag
f	nondimensional stream function
g	density ratio
H	total enthalpy
h	heat transfer film coefficient
L	distance of the step from the leading edge
l	step height
M	mach number
P	temperature or velocity in the non-similar solution
p	pressure
p_t	total pressure
ρ	heat transfer flux
r	radial coordinate
S	injection slot height
T	temperature
t	time
U	velocity
u	x-component of velocity
v	y-component of velocity
α	wedge angle of the body
γ	cooling effectiveness defined in Fig. 12
δ	boundary layer thickness
δ_B	angle of the body
δ_{eq}	angle of the equivalent body
ϵ	eddy viscosity
ϵ_o	constant in the definition of ϵ
θ	angular coordinate

η	similar variable
λ	Mass flow ratio = $\frac{\rho_j U_j}{\rho_e U_e}$
ρ	density
σ	angle of the shock
χ	coordinate defined in Fig. 12
ψ	stream function

Subscripts

j	jet conditions
∞	infinite conditions
e	external conditions
1	higher momentum stream in the similar solution
1	lower momentum stream in the similar solution
ad	adiabatic
w	wall
o	stagnation

LIST OF FIGURES

FIGURE		PAGE
1	Flow fields produced by jets issuing into an oncoming supersonic stream	27
2	Flow field produced by a forward facing step	28
3	Flow field produced by upstream injection along the wall: subsonic injection	29
4	Shadowgraphs a) Model II $M_j = 0.9$ $\frac{s}{\ell} = 0.328$	30
	b) Model VII $M_j = 1.35$ $\frac{s}{\ell} = 0.152$	30
5	Flow field produced by upstream injection along the wall: supersonic injection	31
6	Shadowgraphs a) Model I $M_j = 3$ $\frac{s}{\ell} = 1$	32
	b) Model VII $M_j = 1.4$ $\frac{s}{\ell} = 0.152$	32
7	Experimental model	33
8	Step and slot configurations investigated	34
9	Model instrumentation locations	35
10	Distributions of measured quantities along the wall between the leading edge and the injection slot	36
11	Distributions of measured quantities along the wall between the leading edge and the injection slot	37
12	Distributions of measured quantities along the wall between the leading edge and the injection slot	38
13	Distributions of measured quantities along the wall between the leading edge and the injection slot	39
14	Distributions of measured quantities along the wall between the leading edge and the injection slot	40

FIGURE		PAGE
15	Distribution of measured quantities along the wall between the leading edge and the injection slot	41
16	Distributions of measured quantities along the wall between the leading edge and the injection slot	42
17	Distributions of measured quantities along the wall between the leading edge and the injection slot	43
18	Distributions of measured quantities along the wall between the leading edge and the injection slot	44
19	Distributions of measured quantities along the wall between the leading edge and the injection slot	45
20	Distributions of measured quantities along the wall between the leading edge and the injection slot	46
21	Distributions of measured quantities along the wall between the leading edge and the injection slot	47
22	Distributions of measured quantities along the wall between the leading edge and the injection slot	48
23	Separation and reattachment points as a function of jet Mach number	49
24	Table of geometrical parameters	50
25	Correlation of the results	51
26	Cooling effectiveness	52
27	Dividing streamline angle as a function of the step and slot heights	53
28	Similar solution; nondimensional velocity profile	54
29	Similar solution; nondimensional normal velocity profile	55
30	Similar solution; nondimensional stream function profile	56

FIGURE		PAGE
31	Similar solution; nondimensional velocity profiles	57
32	Similar solution; nondimensional normal velocity profiles	58
33	Similar solution; nondimensional stream function profiles	59
34	Similar solution	60
35	Non-similar solution; velocity profiles distribution	61
36	Non-similar solution; velocity profiles distribution	62
37	Cooling effectiveness; experimental and theoretical results	63
38	Locally similar solution; velocity profiles distribution	64
39	Geometry and boundary conditions for the internal heat conduction problem	65
40	Temperature and equivalent body slope distribution	66
41	Body shapes used for comparing total pressure bodies	67
42	Drag coefficients ratio of two different cooling streams	68

1. INTRODUCTION

The reduction of large total pressure losses across a bow shock in high number flows about blunt bodies is essential in applications where the system's overall efficiency must be maintained relatively high. This requirement suggests the use of bodies with sharper leading edges, and therefore, higher heat transfer rates near the stagnation point. Various methods of leading edge cooling without a corresponding large increase in leading edge radius have been utilized in the past. The most common of these are active cooling by injection at the tip, and regenerative cooling from the inside. However, in both cases, the leading edge radius, or the effective radius, is relatively large and results in pressure losses. To minimize these shock losses, an alternate cooling scheme has been considered here. This scheme reduces these losses by utilizing a small leading edge radius, while at the same time maintaining the tip temperature at an acceptable value.

The proposed system used a cold air counter flowing (upstream injection) jet directed toward the leading edge along the outside surface of the skin of the body. This stream serves to cool the tip and the lateral surface. In the latter, the heat transfer rate is reduced due to the lower stagnation temperature of the cooling stream. Under certain injection conditions, the coolant stream can reach very near the tip region. The tip is then cooled by internal heat conduction from the hot stagnation point region to the lateral surface. The lateral surface, and therefore the tip, are kept below a desired temperature without excessively increasing the equivalent radius of the tip. In Ref. 11 a scheme for supplying the needed cooling air is suggested. An experimental and theoretical investigation has been conducted. This investigation consists

of a qualitative study of the interaction of an upstream injection along a wall with the mainstream, and of a quantitative study to find the optimum conditions for this scheme and the maximum efficiency of the cooling. The purpose of this paper is to present the results of this investigation.

2. DESCRIPTION OF THE PHYSICAL PHENOMENA - GOVERNING PARAMETERS

The flow field resulting from the upstream injection through a wall slot on a forward facing step, incorporates several characteristics of the simpler flow fields which will be described. It is necessary to review these general situations to gain some qualitative insight into the present phenomena.

In Fig. 1a, a flow field produced by a subsonic jet issuing into a counter main-stream is depicted. In this case the main features of the flow are a bow shock across which the main stream decelerates and an interface that separates the jet flow from the main flow. In Fig. 1b, the jet Mach number is supersonic. An experimental investigation of this type was undertaken in Ref. 1. A second shock system associated with the injectant forms, to permit the supersonic jet stream to flow in the opposite direction to the main-stream. On the centerline the total pressure across the dividing streamline must be the same: $p'_{t\infty} = p'_{tj}$ and the position of the dividing streamline is found by imposing this condition.

The jet total pressure must decrease from the value in the nozzle to the value on the dividing streamline, in order to balance the main stream total pressure through the dissipative effect of viscosity. This viscous dissipation can be distributed as in the mixing process or concentrated as in the shock if the stream is supersonic.

In Fig. 2, the flow field produced by a forward facing step is shown

schematically. An experimental investigation of this type of flow was developed in Ref. 2 and 3. Here a separation or dead water region forms an effective wedge to reduce the abrupt body shape and thereby to permit the boundary layer to flow downstream. As in the previous case a dividing streamline separates two regions of the flow field which in this case are the dead water region and the main flow. The position of the dividing streamline depends on the properties of the boundary layer of the main stream (turbulent or laminar boundary layer) and on the shape of the body. In the present investigation the phenomena can be seen to be somewhat of a composite of the above flows. The flow field resulting from the upstream injection along a wall into a supersonic main-stream is illustrated for a subsonic jet in Fig. 3 for a supersonic jet in Fig. 5.

As is the case for free upstream injection (Fig. 1) the shape and the position of the dividing streamline between the two flows is the essential feature of the flow field. This separation line is inclined downstream due to the large difference in the mass flows of the two streams. For supersonic injection, there is also a secondary jet shock to permit the supersonic jet stream to flow in the opposite direction. In this case there is, therefore, a shock - boundary layer interaction due to the presence of the wall. As is the case for the forward facing step, the boundary layer separates (Fig. 2) since the main-stream has to overcome a large adverse pressure gradient. This is a consequence of the presence of an equivalent body due to the injection and the forward facing step. Overcoming this adverse pressure gradient is assisted by the presence of the boundary layer separation, which

occurs further upstream due to the high total pressure of the jet. For these reasons the present flow field is very different from that of a free upstream injection. In this case also, the position of the dividing streamline is determined from the equality of the total pressures. Because of separation, though, the total pressure of the mainstream at the dividing streamline maximum penetration point is nearly the reattachment pressure. The jet total pressure must, thus, decrease until it reaches this value. The dissipation occurs through the shock and the mixing as in the upstream free jet, but also through the effects of the boundary layer at the wall. If the dissipation is not concentrated at the shock, the distance needed to dissipate the jet kinetic energy increases with increasing jet total pressure. Moreover the jet shock interacting with the wall boundary layer induces a simultaneous turning of all the streamlines (Fig. 5 and 6) impeding the injected flow from penetrating forward along the wall. The ensuing expansion and reverse flow with large radius of curvature, produces a large bow shock slope.

For these reasons it is more efficient, from the point of view of the penetration and cooling, to have a subsonic or low supersonic jet. For the latter, the above is true if the height of the jet is such that the supersonic injectant flow becomes subsonic by viscous dissipation and thus there is no local shock. When the shock is not present, the dissipation is due essentially to the mixing process between the two counter-flowing streams. In this case, the physical phenomena can be schematically explained in the following ways: (Fig. 3 and 4)

a) The injection flow decelerates initially as a result of mixing with the co-flowing stream of the region (2) which is a recirculation region due

to the presence of the step over the exit of the nozzle.

b) The injection flow (1) continues to decelerate by mixing with the main stream (4) and because of the difference in momentum it turns back (3) in the direction of the main stream.

c) The main stream has to overcome the new obstacle presented by the secondary jet, and its boundary layer separates because of the adverse pressure gradient. The large separated region (5) of the main stream exchanges momentum by mixing with the injection flow (1) which is also separated near the stagnation point. The separation region (6) of the injected flow is much smaller than the separated region (5). From this schematic analysis it is evident that the physical phenomena are controlled by the mixing between the two counterflowing streams. The importance of the mixing is connected with the extent of the region (2) (and then of the geometry of the model) and with the characteristic properties of the streams. Therefore, the most important parameters that control the flow field are:

a) The mass flow ratio

$$\lambda = \frac{\rho_j U_j}{\rho_e U_e}$$

b) The geometrical parameters

$$d_1 = \frac{s}{\ell}$$

$$d_2 = \frac{\ell}{L}$$

where the lengths s, ℓ, and L are illustrated in figure 3

c) The properties of the injection flow

d) The properties of the main stream

3. APPROACH TO THE STUDY

The purpose of this system is to cool the leading edge of a body without excessively increasing the total pressure losses through the bow shock.

In order to cool the body it is necessary to have:

a) a deep penetration of the coolant jet, and therefore (for the same total jet pressure) a high slot step,

b) a large coolant mass flow.

However, to have low total pressure losses, a small shock slope is necessary; that is possible if:

a) the jet mass flow is small

b) the height of the step is small

The conditions for cooling the body and minimizing pressure losses are contradictory, and the optimal conditions must be found by varying the parameters of the flow field. An experimental analysis was conducted first in an effort to clarify the phenomena and to find the optimum conditions for the system. A theoretical analysis was then developed in order to calculate some particular aspects of the flow field.

4. EXPERIMENTAL INVESTIGATION

a) Experimental Equipment: The Mach 6 Blowdown wind tunnel at the NYU Aerospace Laboratory was utilized. This tunnel is capable of achieving stagnation pressures of 2000 psia, and of exhausting into a vacuum sphere with a few millimeters of mercury for back pressure; the wind tunnel has a

test section diameter of 12". It can also achieve a stagnation temperature of 900°R. For this series of experiments, the stagnation pressure was maintained at 1000 to 1200 psia and the stagnation temperature was maintained in the range of 600-900°R.

b) Model: A two-dimensional wedge was used. (Fig. 7) The model was instrumented with thermocouples and pressure taps on both surfaces. It had a slightly blunt leading edge of 1/32" radius. The wedge half-angle was 4° and 3" wide injection chambers were built above the upper and lower surfaces of the wedge.

The injection chambers were designed to have interchangeable nozzles: this enables the model to vary the parameter M_j (changes in injection stagnation pressure to lower values would also change M_j to either subsonic or a "shock-down" lower supersonic Mach number)

Two nozzles were used: (Fig. 8)

1. Nozzle I, designed for M=3 injection, used for high supersonic injection.
2. Nozzle II, designed for M=1.3 injection, used for low supersonic or high subsonic injection. It was determined that a nozzle which achieved M=1 in the throat is necessary for steady subsonic upstream injection. In fact if the injection stagnation pressure is low enough to have subsonic flow throughout the injection chamber, oscillations in injection would occur causing oscillations in the pressure and mass flow of the injection. Therefore, in order to avoid this

undesirable condition and still maintain subsonic flow at the nozzle exit, the injectant stagnation pressure had to be adjusted in order to achieve M=1 at the throat. The flow is then shocked down to a subsonic value at the exit of the nozzle.

In addition, it was possible, by the addition of shims, to vary the height of the exit section of the nozzle. Various "steps" could also be added. Since the exit height and the height of the step could be varied, it was possible to test with different values of the parameters $\frac{s}{\ell}$, and $\frac{\ell}{L}$. The injectant was air, which was cooled by being pumped through a coil of tubing immersed in a bath of liquid nitrogen. It was possible to achieve injectant air temperatures in the range of 250-350°R, and to vary the temperature by changing the amount of coil immersed in the liquid nitrogen. Therefore, as a result of the methods just described, it was possible to vary the following: the temperature of injection, the exit section and step height of the nozzle $\left(\frac{s}{\ell}\ \frac{\ell}{L}\right)$, and the Mach number M_j. As a result, different values of the parameter λ were obtained.

The model is shown (Fig. 7) with the Mach 3 nozzle mounted and no additional step at the exit. In Figure 8, the various step and nozzle configurations are shown. In Figure 9, the layout of pressure taps and thermocouples on the upper and lower surfaces of the wedge is depicted.

c) Measurements: For a quantitative and a qualitative analysis of the physical phenomena occuring in these experiments it was necessary to measure:

1) The pressure distribution between the leading edge and the step.

2) The heat transfer and temperature distribution along the same surface.

3) The exit conditions of the injectant air.

In order to measure the pressure dsitribution, the pressure orifices were placed as shown in Fig. 9. The 11 orifices are connected to a scanning valve which is in turn connected to a 0 to 10 psia transducer. The output of the transducers was placed on a Visicorder. In order to measure the heat transfer distribution and the adiabatic temperature distribution, the transient method is used utilizing the thin skin technique. It is interesting to note that for this surface the steady state temperature is not the adiabatic temperature because heat conduction inside the body is always present in the problem under consideration. The adiabatic temperature distribution has to be known to impose the boundary condition in the solid heat conduction problem that gives the steady state temperature distribution inside the body. The transient method requires the thermocouples to be welded to the inside surface of a shimstock (in the present case .020" stainless steel) which is then mounted flush to the wedge surface. (Fig. 9) The thermocouples are connected to the Visicorder Oscillograph, which gives the temperature as a function of time. Therefore the slope $\left(\frac{dT}{dt}\right)$ can be measured from the Visicorder recording of each test. Before discussing how the heat transfer is calculated, corrections must be made in order to take care of the effects of heat conduction within the shimstock to which the thermocouples are welded. All of the changes in temperatures measured by the thermocouples are due not only to the effects of aerodynamic heating and injectant cooling, but also due to heat conduction in the shimstock. As a result, a heat conduction correction must be introduced. This heat conduction correction increases with respect to the time dependent heat capacity term as time increases. Since this correction term always brings some error of computation, it is better to measure slopes $\left(\frac{dT}{dt}\right)$ for small times. For any test, if only the heat transfer is desired, measurements are taken a very short time

after the test is started. From the heat transfer, if the temperature difference is known, it is then possible to calculate the value of the heat transfer coefficient h from Newton's Law of Cooling:

$$\dot{q} = h\Delta T$$

In the problem being studied, ΔT is unknown because the local adiabatic temperature along the wall depends on the mixing between the injectant air and the main stream. As a result, it is necessary to measure the slope at 2 successive points in time for each curve (thermocouple). The two points are taken near the starting of the tunnel in order to minimize the effects of heat transfer in the shimstock. With the hypothesis that h is constant in the range of temperature it is possible to determine h and the adiabatic temperature distribution for each thermocouple position at the lateral surface. In slot cooling experiments, the transfer measurements by the transient technique, as used in here, was shown (Ref. 4) to give slightly higher adiabatic wall temperature than would be directly measured in a long time wind tunnel. The adiabatic wall temperature values computed with the transient technique are conservative in terms of the absolute cooling flow needed to maintain the surface below a certain temperature. Therefore the direct adiabatic temperature measurements give greater values of the cooling efficiency. The same errors in the measurements could arise in the present experiments also, and for the reasons illustrated above the adiabatic wall temperature values computed could be slightly inaccurate but on the conservative side. In order to measure the exit conditions of the jet, three probes were built into the injection chamber and injectant nozzle. A thermocouple was installed in the nozzle and connected to pressure transducers. From these measurements the M_j and mass flow were determined.

d) Tests Results: The dependence of the flow field characteristics on the injection Mach number has been considered first because the flow pattern that

is established depends more critically on the value of the injection M than on the other parameters. In fact a completely different flow pattern has been observed in the range of Mach numbers explored. In Figures 10 to 22, the results for different M_j are shown on various main stream conditions. For all tests, the results consist of:

a) shadowgraph

b) pressure distribution

c) heat transfer distributions

d) adiabatic temperature distribution

From a and b, it is possible to determine the slope of the shock. From a, b, and c, it is possible to determine the point of separation on the wall and the point of reattachement of the main stream. These data are plotted as a function of Mach number in Figure 23.

From the results of this series of tests, it is clear that the optimal performance of this system is for values of M_j near unity. The influence of the other three parameters λ, $\frac{s}{\ell}$, $\frac{\ell}{L}$ on the efficiency of the system has been consequently analyzed. The variation of these three parameters is achieved, keeping M_j at the optimum value previously determined. In Figure 24 a table with the values of the geometrical parameters in all the models used is presented, and the tests corresponding to those models is shown. The results show (Fig. 10-22) the penetration of the jet increases with increasing values of the geometrical parameters $\left(\frac{\ell}{L}\right)$, $\left(\frac{s}{\ell}\right)$ and of the mixing parameter λ. In fact, increasing the total height of the step $\left(\frac{\ell}{L}\right)$ for the same value of $\left(\frac{s}{\ell}\right)$ the length of the region (2) of mixing between the coflowing streams increases. Increasing the height of the slot $\left(\frac{s}{\ell}\right)$ for the same value $\left(\frac{\ell}{L}\right)$ the jet mass flow increases, and a larger distance in needed to dissipate the larger kinetic

energy of the jet. As these geometrical parameters increase, the slope of the bow shock is seen also to increase. Therefore, a compromise value must be chosen for these parameters.

Also if the parameter λ increases (as a result of higher M_j, or lower T_{oj}) within the aforementioned limits, the penetration of the jet increases. All the results are correlated in b). It is interesting to note from the pressure diagrams that downstream of the usual separation pressure distribution, a second pressure plateau appears (Fig. 11, e.g.). This plateau occurs in the mixing zone of the two counterflowing streams. Therefore, this mixing may be assumed to take place at approximately constant pressure.

e) Correlation of Data: It is possible to correlate all the experimental results shown in d). The effectiveness, γ, has been defined for this purpose (Ref. 5):

$$\gamma = \frac{T_{aw} - T_{o\infty}}{T_{oj} - T_{o\infty}}$$

The variation of γ with the parameters s/ℓ, ℓ/L and λ (for the optimum value of M_j) was examined. A correlation for γ was found as a function of a product of powers of the main parameters

$$\chi = \left(\frac{x}{s}\right)^{0.75} \left(\lambda\right)^{-1.50} \left(\frac{s}{\ell}\right)^{0.45}$$

The exponents in the above expression were determined from logarithmic plots of γ versus each parameter at constant values of the other two, as shown in Fig. 25 for example. The validity of the suggested correlation extends over the complete range of the measured values.

Plotting γ in this new variable, a very regular trend was obtained agreeing with a power law relationship as follows.

$$\gamma = C - K\chi \qquad \text{(Fig. 26)}$$

This says that γ decreases with increasing x/s, $1/\lambda$, s/l. When these results are compared with the correlations of results for downstream injection, it is found that the power of (x/s) is of lower degree and the power of λ is of higher degree. This difference can be explained by the fact that in upstream injection, the mixing of the injectant with the main stream occurs via the reverse flow of the injectant itself. Therefore, up to the point where the injectant jet penetrates, the influence of x/s on γ is less, and the influence of λ is greater. Although the validity of this law is obviously limited to the examined range, it is possible to find in that range, or with small extrapolations, the values of ϵ for flight conditions, and different values of λ, s/ℓ, ℓ/L. (Fig.26) An extrapolation for different free stream Mach number (M=6 to 8) was also done; however, the approximation of these results is obviously much less accurate (Fig.28). The shock slope was also correlated: a correlation $\sigma-\delta_B$ with ℓ as a parameter is shown in (Fig. 27). It is possible to see from the diagram that $(\sigma-\delta_B)$ (where δ_B is the body angle) increases with ℓ and that there is an optimum value for (s/ℓ). There was not enough data to express a law of correlation. In any case, it is physically evident that σ increases with (ℓ/L). The increasing of s at first results in decreasing the slope of the equivalent body in comparison to the slope of the separation line caused by the step. Then if the mass flow is too large, the slope increases.

5. THEORETICAL ANALYSIS

Following the flow field model observed in Section 2, the mixing between two counterflowing streams essentially governs the structure of the flow field

under consideration, if the upstream jet is subsonic or low supersonic. Therefore, this region of the flow field is amenable to theoretical analysis. The intent here is to obtain results which will be compared with experimental measured quantities.

a) Basic Equations and Hypothesis: The mixing region can be analyzed with the usually adopted boundary layer approximation. From the conclusion of 5a, the pressure can be assumed constant in the region of interest, as a first approximation. With this hypothesis, the conservation equations for turbulent compressible, homogeneous flow, can be written (Ref. 6) if Pr is considered to be equal to one

$$\frac{\partial \rho u}{\partial x} + \frac{\partial \rho v}{\partial y} = 0 \tag{1}$$

$$\rho u \frac{\partial u}{\partial x} + \rho v \frac{\partial u}{\partial y} = \frac{\partial}{\partial y}\left(\rho \varepsilon \frac{\partial u}{\partial y}\right) \tag{2}$$

$$\rho u \frac{\partial H}{\partial x} + \rho v \frac{\partial H}{\partial y} = \frac{\partial}{\partial y}\left(\rho \varepsilon \frac{\partial H}{\partial y}\right) \tag{3}$$

where the quantities are the time averaged flow properties. The boundary conditions will be specified below.

The flow field in the mixing region is essentially non-similar due to the jet velocity decay on the upstream direction. A locally similar analysis was conducted by combining:

1. a non-similar solution, essentially valid near the wall in the jet region which takes into account the upstream velocity decay

of the jet flow and

2. a station by station similar solution dependent on the local external stream conditions.

b) Similar Solution: Under the similarity assumption the new dependent and independent variables are introduced as usually (Ref. 6)

$$\eta = \frac{y}{x}\,\epsilon_o^{-\frac{1}{2}}$$

$$f = \int_o^n \frac{\rho u}{\rho_1 u_1}\, d\eta$$

$$\psi = \rho_1 u_1\, x \epsilon_o^{\frac{1}{2}}\, f(\eta)$$

where $\rho\epsilon = \epsilon_o u_1 \rho_1\, x$ and ϵ_o will be defined below when the eddy viscosity model is chosen. The subscript 1 and 2 denote the higher and lower momentum external streams and x is measured from the upstream penetration point. The energy equation in the form 3) admit the Crocco's integral and the density ratio can be expressed by

$$g = \frac{\rho_1}{\rho} = \left[1 + B\left(\frac{u}{u_1} - 1\right) - C\left(\left(\frac{u}{u_1}\right)^2 - 1\right)\right]$$

where $$B = \frac{1-H_{21}}{1-u_{21}}\left[1 + (\gamma-1)\frac{M_1^2}{2}\right], C = (\gamma_1-1)\frac{M_1^2}{2}$$

In these variables, using the integral of the energy equation, the unknown function f is determined from the following equation

$$\left(\frac{(f'g)'}{g}\right)' + f\,(f'g)' = 0 \qquad (4)$$

In order to define the appropriate boundary conditions for this third order

ordinary differential equation, it is necessary to examine the physical problem under consideration. The flow field due to the mixing between two counterflowing streams (the main flow and the jet) was investigated neglecting as a first approximation the effect of the wall boundary layer. When mixing occurs between counterflowing streams one of them must be considered finite, since all the lower momentum stream is reversing is in the direction of the higher momentum stream.

Three boundary conditions must be imposed; two of them are the usual boundary conditions at infinity and at the axis y = 0, the third boundary condition is imposed where the stream function is again zero, instead of infinity as in coflowing streams. The last is imposed at a free boundary η_o determined from the following integral equation

$$f = \int_o^{\eta_o} \frac{\rho u}{\rho_1 u_1} \, d\eta = 0 \tag{5}$$

Specifically the boundary conditions to be applied are, if the wall is considered a streamline

$$\eta \to \infty \qquad u = u_1 \tag{6}$$

$$\eta = 0 \qquad \psi = 0 \tag{7}$$

$$\eta = \eta_o \qquad u = u_2 \tag{8}$$

This equation and boundary conditions were solved numerically using a quasi linearization method of the system. (App. I)

$$u = gf' \tag{9}$$

$$gu'' - g'u' + g^2 f u' = 0 \tag{10}$$

$$g = 1 + B\,(u-1) - C(u^2-1) \tag{11}$$

and 5) 6) 7) and 8. Numerical results are shown in Fig. 28-33 for different ratios of u_1 to u_2.

The velocity profiles are different from the coflowing streams case, in particular they are much more extended in the negative η side, and consequently also the value of the normal velocity component v is much larger, as can be expected because of the reverse flow.

Imposing the condition that the wall is the zero streamline (f=0 in the negative side of η) (Fig. 34), it was possible to find the position of the zero streamline ($f = 0$, $\eta = 0$) or dividing streamline. In fact if the u and v profile are know, the dividing streamline slope with respect to the new reference of the wall can be found in the transformed plane. In order to transform back to the physical plane it is necessary to define the value of ε_o that means to specify the eddy viscosity model.

c. Non-Similar Solution: The above similar solution cannot take into account the influence of the initial profile and cannot give the decay of u_j with the upstream distance from the jet. To improve the solution the non similar problem must be considered. To investigate this problem an approximate analytical method was used. The improved Oseen linearization of the boundary layer equations (Ref. 7) on the physical plane.

The same linearization, on the Von Mises plane, that gives a slightly more accurate solution, could not be used in the present problem because of the reverse flow that gives a double value profile in ψ. Accordingly to that linearization the convective derivative

$$\rho u \frac{\partial P}{\partial x} + \rho v \frac{\partial P}{\partial y} = (\rho u)^* \frac{\partial P}{\partial x}$$

where P is u or T, the momentum or energy equation are reduced to the form

$$(\rho u)^* \frac{\partial P}{\partial x} = \frac{\partial}{\partial y}\left(\rho\epsilon \frac{\partial P}{\partial y}\right) \tag{12}$$

where $(\rho u)^*$ is an approximate average value to be found in such a way that the approximation gives the minimum error.

If a model for the eddy viscosity is used for which $\rho\epsilon$ is only a function of x, the equation (12) can be put in the heat equation form

$$\frac{\partial P}{\partial \xi} = \frac{\partial^2 P}{\partial y^2} \tag{13}$$

where $$\xi = \int_0^x \frac{\rho\epsilon}{(\rho u)^*}\, dx \tag{14}$$

This is a parabolic linear partial differential equation and can be solved in closed form. The boundary condition for this problem is:

a specified initial condition

$$P(0,y) = w(0,y) \tag{15}$$

two boundary conditions

$$\lim_{y \to \infty} P = P_e \tag{16}$$

and $$y = 0 \qquad \frac{\partial P}{\partial y} = 0 \tag{17}$$

if the wall is considered a centerline streamline of a symmetric flow field as a first approximation, when the wall boundary layer is thin compared to the entire mixing zone. The solution of the temperature field with the

second boundary condition (17) is adoptable when considering an adiabatic wall as was nearly the case with the thin skinned model used in the present experiments. The present condition (17) was selected because the intent was first to compare the theoretical results with the experimental values, and once agreement is obtained the theory may be applied to different conditions. In the actual case, i.e. solid body, in y = 0 a different boundary condition consistent with the internal heat conduction problem must be imposed (see Section 6). With these approximations, the solution was found in the transformed plane (ξ,y) for different initial conditions (velocity and temperature profiles and step heights) the solution of equation (13) is (Ref. 8)

$$P(\xi,y) = P_e + \int_0^\infty [w(y') - P_e]\, G(y,y',\xi)\, dy' \tag{18}$$

Where $G(y,y',\xi)$, the Green function associated with the system, is

$$G(y,y',\xi) = \frac{1}{2\pi\xi} \left[e^{-\left(\frac{y+y'}{2\xi^{1/2}}\right)^2} + e^{-\left(\frac{y-y'}{2\xi^{1/2}}\right)^2} \right] \tag{19}$$

The momentum and energy equation are formally identical, then considering the different boundary conditions, the same kind of solution is valid for both fields. In App II are reported some solutions for different initial conditions. From the temperature, the density distribution is determined. The results shown in Figs. 35-36 are in the transformed plane (ξ,y). In order to transform them in the physical plane with

$$x = \int \frac{(\rho u)^*}{\rho\varepsilon}\, d\xi \tag{20}$$

$(\rho u)^*$ must be chosen. Many choices are possible, but in order to have good approximation in the jet region,

$$(\rho u)^* = \rho_j u_j\ (x)$$

must be used. With this value and $\rho\epsilon$, defined below, the value of the physical coordinate was computed and the flow field in the physical plane was then obtained.

d. Locally Similar Solution: A combination of the nonlinear similar solution and the linearized non-similar solution was performed.

With the above choice for $(\rho u)^*$ the linearized solution is not strictly valid far away from the jet. Therefore to overcome this shortcoming the linearized solution was used as a guide in selecting the similar profile valid at each particular axial station by matching the u_1 of the similar solution with the centerline velocity $u(x,o)$ of the non-similar solution. In this way, it is possible to describe the entire flow field station by station, using the concept of local similarity.

To obtain the flow field in the physical plane the eddy viscosity, previously assumed to be a function of x only, in the linearized solution, and more specifically a linear function of x in the similar solution, must be defined explicitly. The model, usually selected for high speed compressible jet mixing problems (Ref. 8)

$$\rho\epsilon = ky^{\frac{1}{2}} [(\rho u)_2 - (\rho u)_1] \tag{21}$$

was assumed. In (21) k is a constant and $y^{\frac{1}{2}}$ is the height in the mixing zone in the physical plane where the quality ρu has an average value between the two streams. Results from the locally similar solution were compared with the experimental results. In particular the shape of the dividing streamline and the value of the parameter γ, defined in (Section 4e) were compared. Figures 37-38 show good agreement between experiment and theoretical calculations.

Other theoretical eddy viscosity models may be used to obtain better agreement. Alternatively, an ad hoc semi-empirical model can be obtained from the present experiments for extrapolation to similar experiments but under different flow conditions.

6. COMPUTATION OF THE TEMPERATURE FIELD INSIDE THE BODY

Aerodynamic heating of a leading edge occurs, in reality, through skin friction deceleration of the external hypersonic stream and cooling internally by heat conduction. To find the temperature field of the solid body, therefore, the heat conduction problem and the aerodynamic problem must be solved simultaneously since at steady state the two phenomena occur at the same time and at rates that maintain steady state conditions.

Therefore, the boundary conditions at the interface of the two problems (i.e. the wall) are unknown to both the external aerodynamic problem and the internal heat conduction problem. This is peculiar to the present problem since the wall temperature is not permitted to reach adiabatic conditions due to the upstream injection cooling. Therefore, the temperature field inside the slightly blunted wedge (see Fig. 39) was obtained solving the heat conduction equation.

$$\nabla^2 T = 0 \tag{22}$$

subject to the boundary conditions

$$\left(\frac{1}{r}\frac{\partial T}{\partial \theta}\right)_w = \frac{h}{k}\left[T_{ad}(r) - T_w(r)\right] \tag{23}$$

or explicitly

$$\left(\frac{1}{r}\ \frac{\partial T}{\partial \theta}\right)_w - \left(\frac{h}{k}\right) T_w\ (r) = \frac{h}{k}\ T_{ad}\ (r)$$

on the external surface

and

$$\frac{1}{r}\ \frac{\partial T}{\partial \theta} = 0 \qquad \theta = 0 \qquad (24)$$

$$T = T_c \qquad r = r_s$$

where τ_s corresponds to the injection section.

Here h and $T_{ad}(\tau)$ are known functions which were obtained from experiments, except in the small nose region where the stagnation point distribution was used (Ref. 10). In the actual case the boundary condition (23) replaces the one imposed in Section 5 (17), thereby coupling the aerodynamic and heat conduction problems in the approximation previously adopted.

As a first approximation an analytical solution of the system (22-24) was derived with a slight simplification of the body geometry as shown in Fig. 39 in order to obtain a body analyzable in cylindrical coordinates. Results for the leading edge temperature are plotted in Fig. 40.

7. APPLICATIONS AND COMPARISONS

The method presented for cooling the leading edge has general applicability when it is necessary to maintain the temperature below a fixed value for high Mach numbers, while at the same time achieving small pressure losses. These conditions are desirable for both supersonic wings and supersonic turbine and compressor blades. (Ref. 11)

A comparison between the total pressure losses and therefore the drag of the frontal part of a body with internal cooling (Ref. 12) and the drag for the

corresponding part of the body which utilizes the system of cooling under consideration was carried out. As shown in Fig. 41 $D = D_{L.E.} + D_w$ where $D_{L.E.}$ is the drag of the leading edge, and D_w is the drag due to the wedge portion. A comparison is made between a body which corresponds to a geometry needed for internal cooling with a relatively larger nose radius and a body with a smaller nose radius that corresponds to the equivalent body of the upstream injection and step configuration. This equivalent body is represented by the smaller radius tip and the slip stream formed by the jet and the free stream. Therefore the drag of this equivalent body is the same as that of the physical body, the jet momentum change and the step, since the separation zone is in equilibrium with the surrounding. The smaller nose radius body has a larger afterbody wedge angle, α_2, due to the equivalent body mentioned above. Drag calculations were compared for the portions of the bodies shown in Fig. 41 assuming a Newtonian pressure distribution to be valid. Values of R_1 used are typical of regenerative cooling schemes (Refs. 12-13). R_2 is taken to be equal to .016 inches. The value of α_2 depends, as shown previously, on the value of the parameters λ, $\frac{s}{\ell}$, $\frac{\ell}{L}$. It is evident from Figure 42, that the drag depends strongly on the nose radius and weakly on the angle α_2. From the above results, it is possible to conclude that the major contribution to drag is due to the nose bluntness and due less to the wedge angle α_2. Therefore, the present scheme has less losses. Higher penetration and cooling are possible by increasing λ, $\frac{s}{\ell}$, $\frac{\ell}{L}$. Since the angle of the dividing streamline or equivalent body does not effect considerably the requirement of low total losses.

8. CONCLUDING REMARKS

A leading edge cooling system by upstream injection along the surface, that produces small total pressure losses, has been investigated. A flow field model, for the upstream injection along the wall, was established in order to find the parameters that control the physical phenomenon. An experimental investigation has been conducted to find values of the above parameters to give an efficient cooling scheme from the point of view of upstream jet penetration and minimum shock losses. The results suggest

a) high subsonic or low supersonic injection speed is required

b) large values of the injection mass flow (or λ) and the stepsize (or $\frac{\ell}{L}$) may be used to increase the effectiveness of the cooling, even if the slope of the equivalent body (due to the step and the injection) increases.

A theoretical analysis was performed to study the flow field in the mixing region. The results obtained applying the present analysis to the experimental conditions, compare favorably with the experimental results. It is, therefore, concluded that the approximation made is reasonable, and that the theoretical model is usable for different conditions.

The present study indicates, from comparison with different cooling systems, that for the same leading edge cooling, the present scheme gives less total pressure losses.

The present cooling scheme may be further improved with the aid of a more rigorous theoretical analysis and through experimental investigation of the complete interaction region.

REFERENCES

1. Romeo, David, J. and Sterrett, James R., "Exploratory Investigation of the Effect of a Forward Facing Jet on the Bow Shock of a Blunt Body in a Mach Number 6 Free Stream," NASA TND-1605, 1963.

2. Bogdonoff, S.M. and Kepler, C.E., "Separation of a Supersonic Turbulent Boundary Layer," Report 249, Princeton University, Department of Aeronautical Engineering, January 1954.

3. Sterrett, J.R. and Emery, J.C.,"Extension of Boundary Layer Separation Criteria to a Mach Number of 6.5 by Utilizing Flat Plates with Forward Facing Steps," NASA TND-618, December 1960.

4. Beckwith, Ivan, E., and Bushnell, Dennis, M., "Calculation by a Finite-Difference Method of Supersonic Turbulent Boundary Layers with Tangential Slot Injection," NASA TND-6221, April 1971.

5. Zakkay, V., Sakell, L., and Parthasarathy, K., "An Experimental Investigation of Supersonic Slot Cooling," Proceedings of the 1970 Heat Transfer and Fluid Mechanics Institute, Stanford University Press, Stanford, California.

6. Napolitano, L.G., Libby, P.A., and Ferri, A., "Recent Work on Mixing at the Polytechnic Institute of Brooklyn," PIBAL 435, December 1957.

7. Lewis, J.A. and Carrier, G.F., "Some Remarks on the Flat Plate Boundary Layer," Journal of Applied Mathematics, Vol. II, No. 2, 1949.

8. Carslaw, H.S. and Jaeger, J.C., "Conduction of Heat in Solids," Oxford Press, 1967.

9. Ferri, A., Libby, P.A., and Zakkay, V., "Theoretical and Experimental Investigation of Supersonic Combustion," ARL Report 62-467, September 1962.

10. Lees, L., "Laminar Heat Transfer Over Blunt-Nosed Bodies at Hypersonic Flight Speeds," Jet Propulsion, April 1956.

11. Ferri, A., Fox, H., and Hoydysh, W., "Active Cooling of Hypersonic Airplanes," NASA CR-66930, January 1970.

12. Becker, John V., "New Approaches to Hypersonic Aircraft," presented at the Seventh Congress of the International Council of the Aeronautical Sciences (ICAS), Rome, Italy, September, 1970.

13. McConarty, W.A. and Anthony, Frank, M., "Design and Evaluation of Active Cooling Systems for Mach 6 Cruise Vehicle Wings," NASA CR-1916.

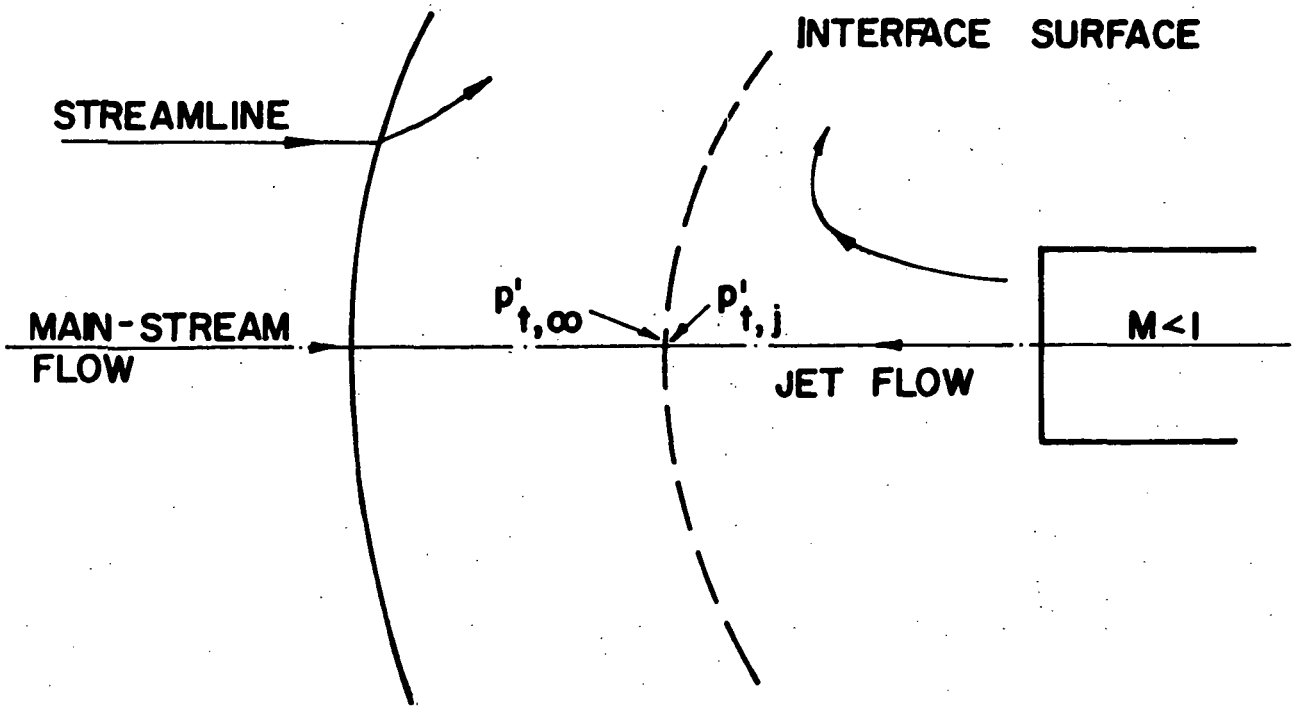

a) SUBSONIC INJECTION

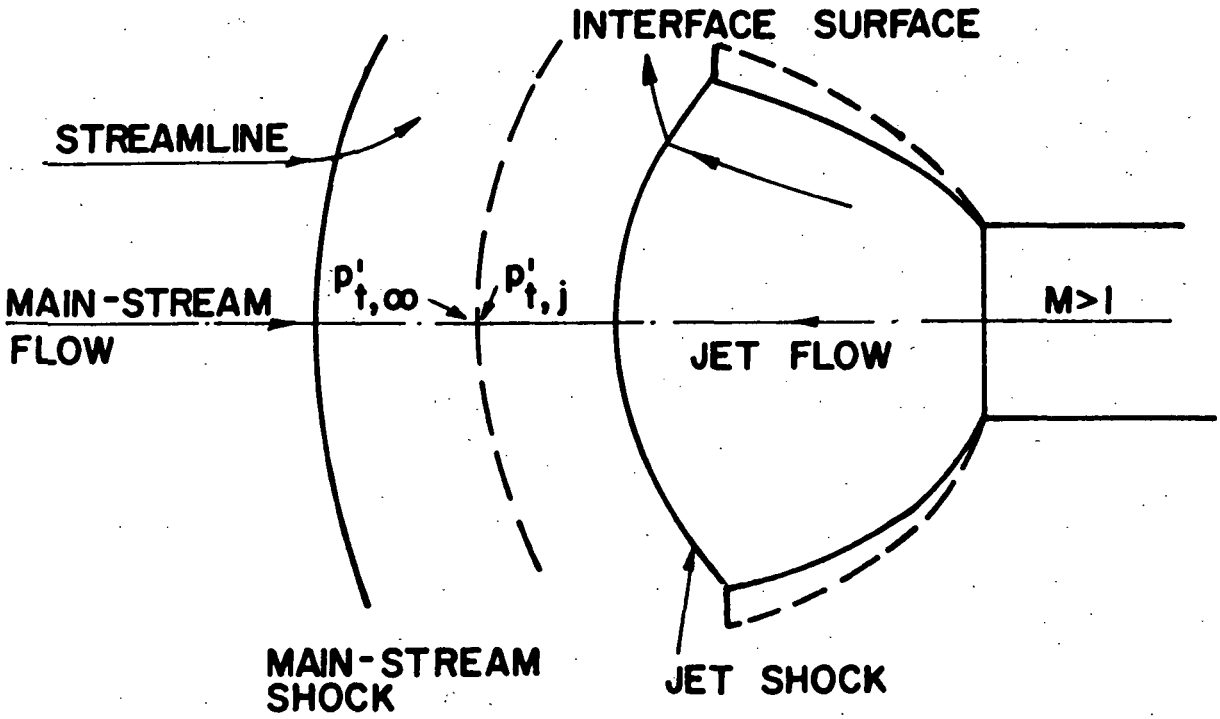

b) SUPERSONIC INJECTION

Fig. 1 Flow fields produced by jets issuing into an oncoming supersonic stream

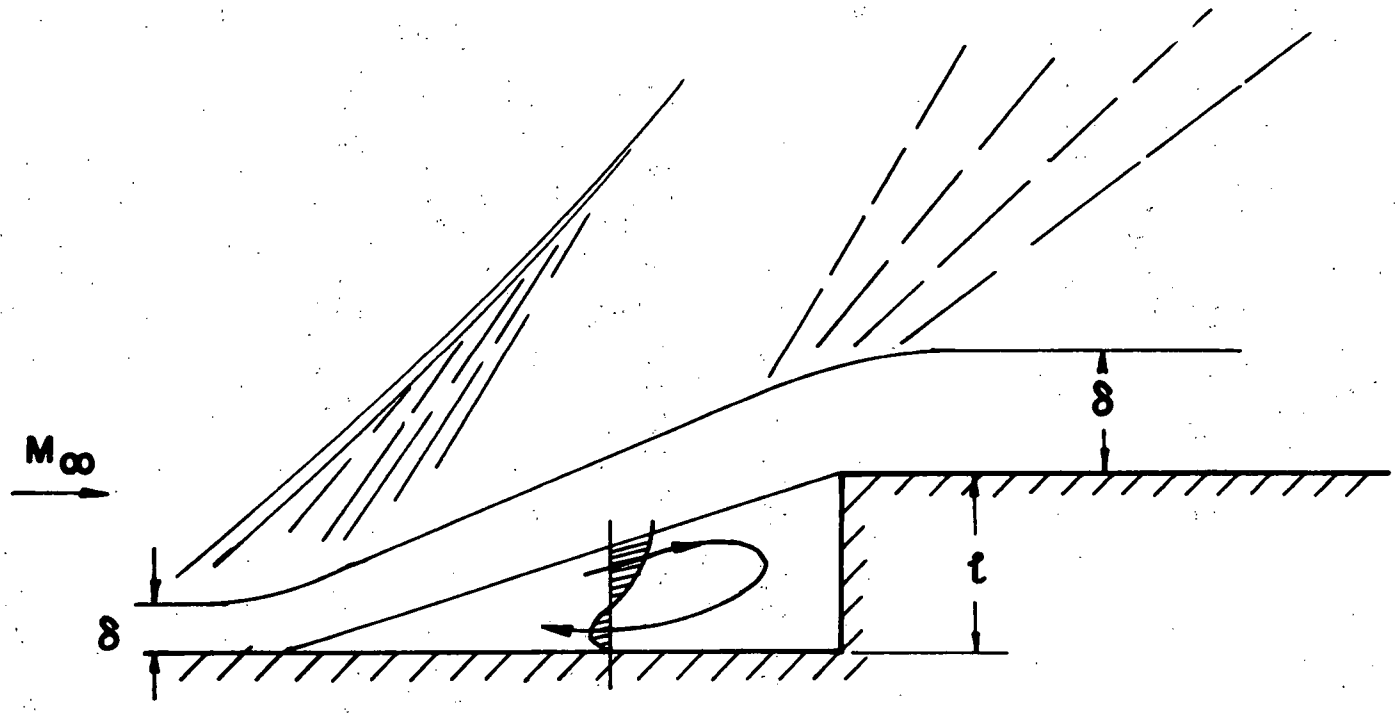

FORWARD FACING STEP FLOWFIELD

Fig. 2 Flow field produced by a forward facing step

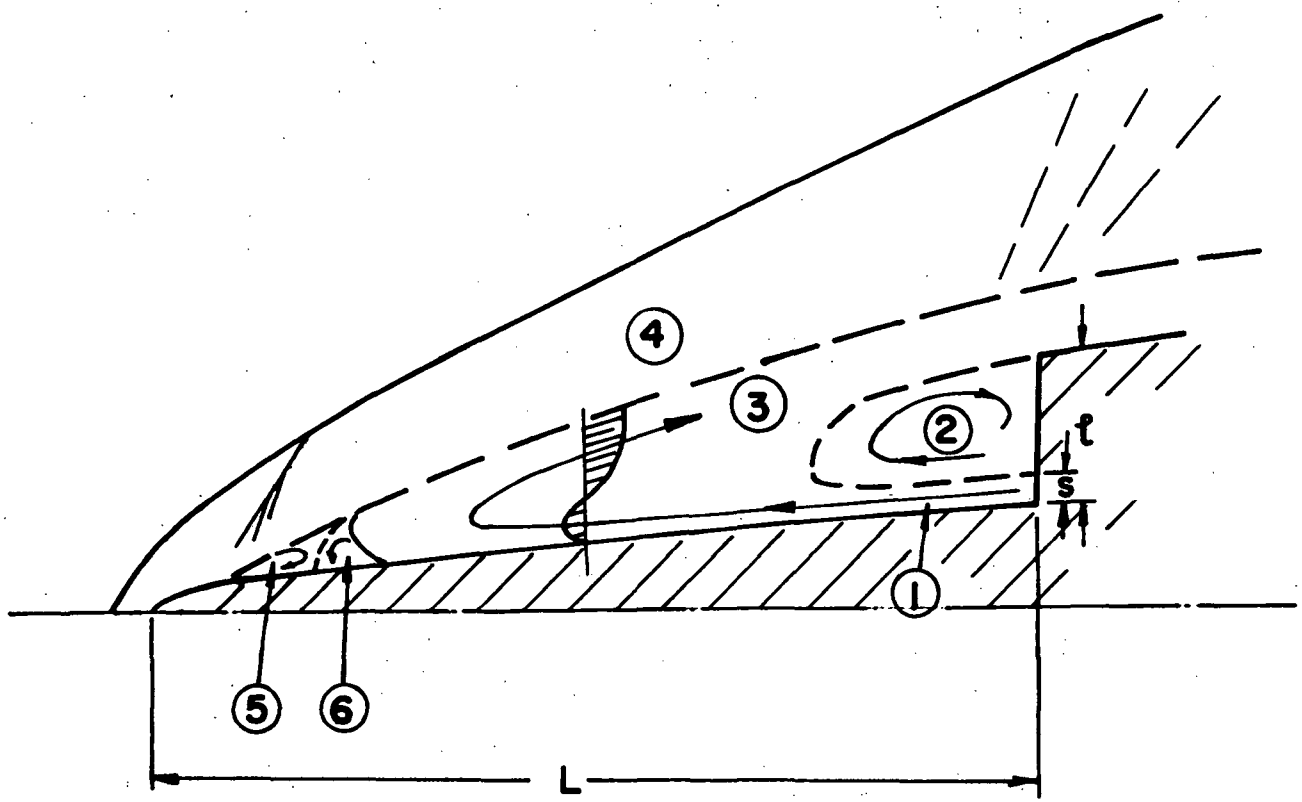

UPSTREAM INJECTION FLOW FIELD

Fig. 3 Flow field produced by upstream injection along the wall: subsonic injection

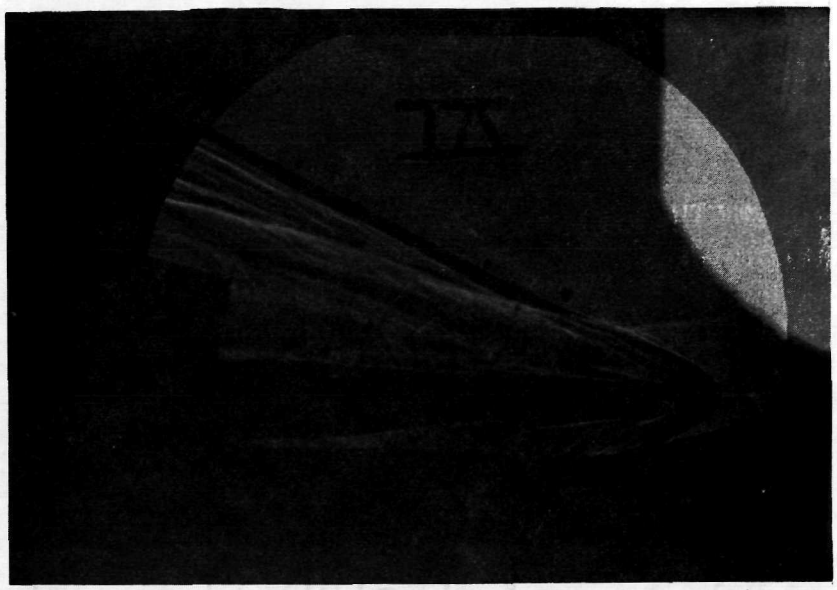

a) Model II $M_j = 0.9$ $\frac{s}{\ell} = 0.328$

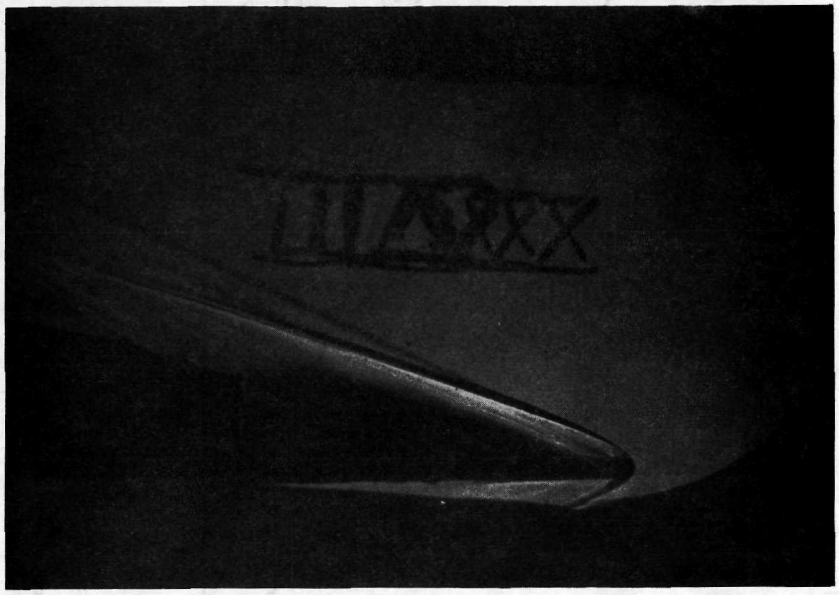

b) Model VII $M_j = 1.35$ $\frac{s}{\ell} = 0.152$

Fig. 4 Shadowgraphs

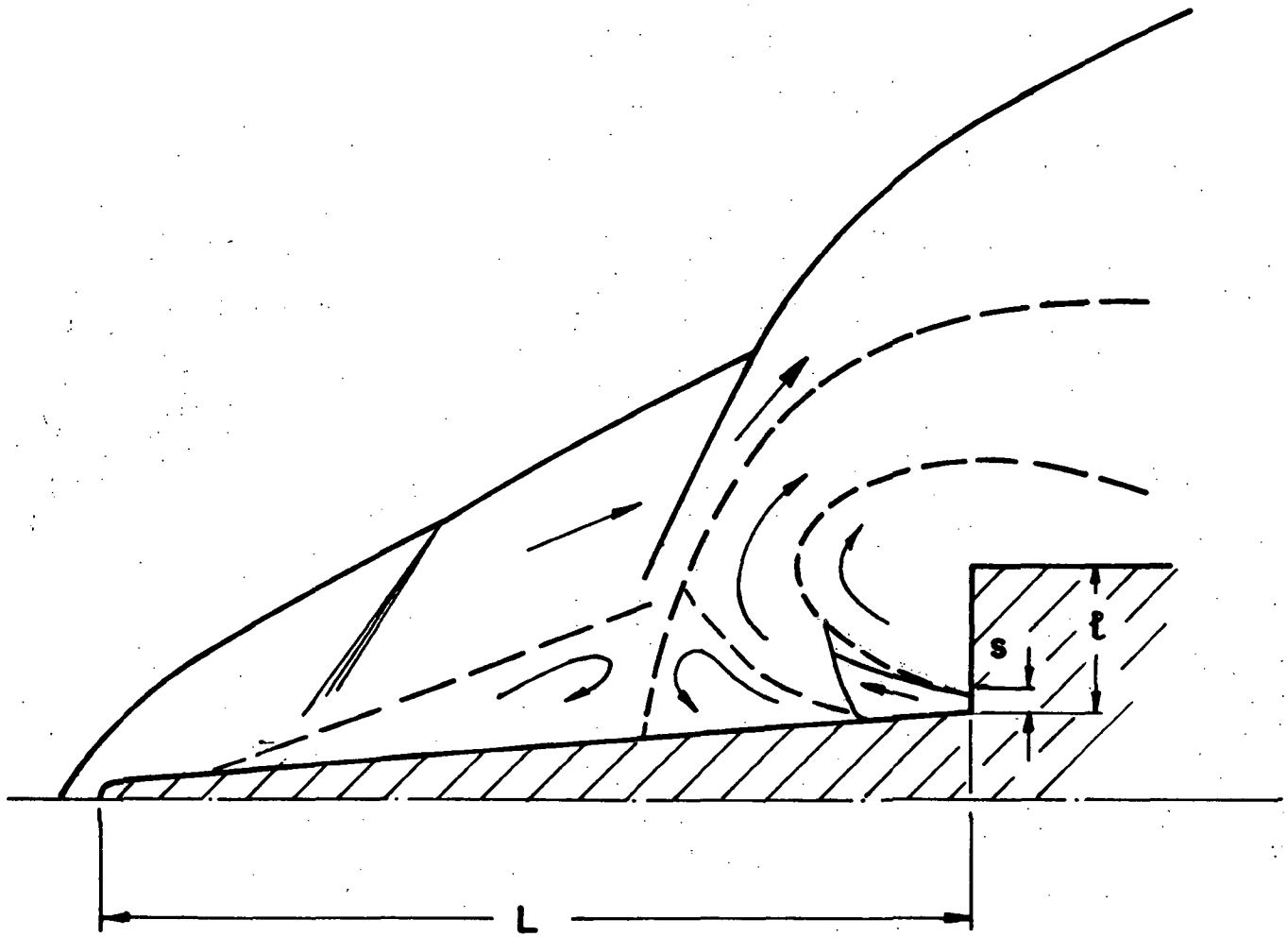

Fig. 5 Flow field produced by upstream injection along the wall: supersonic injection

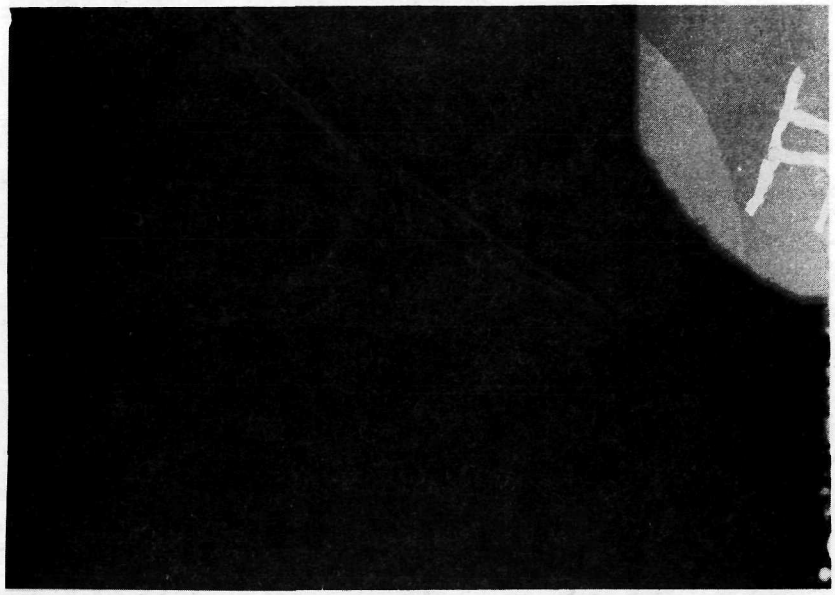

a) Model I $M_j = 3$ $\frac{s}{\ell} = 1$

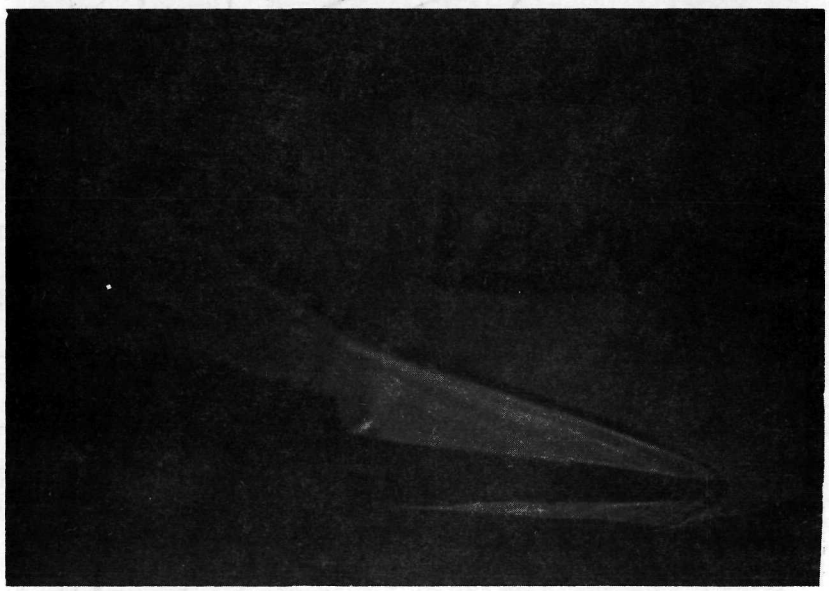

b) Model VII $M_j = 1.4$ $\frac{s}{\ell} = 0.152$

Fig. 6 Shadowgraphs

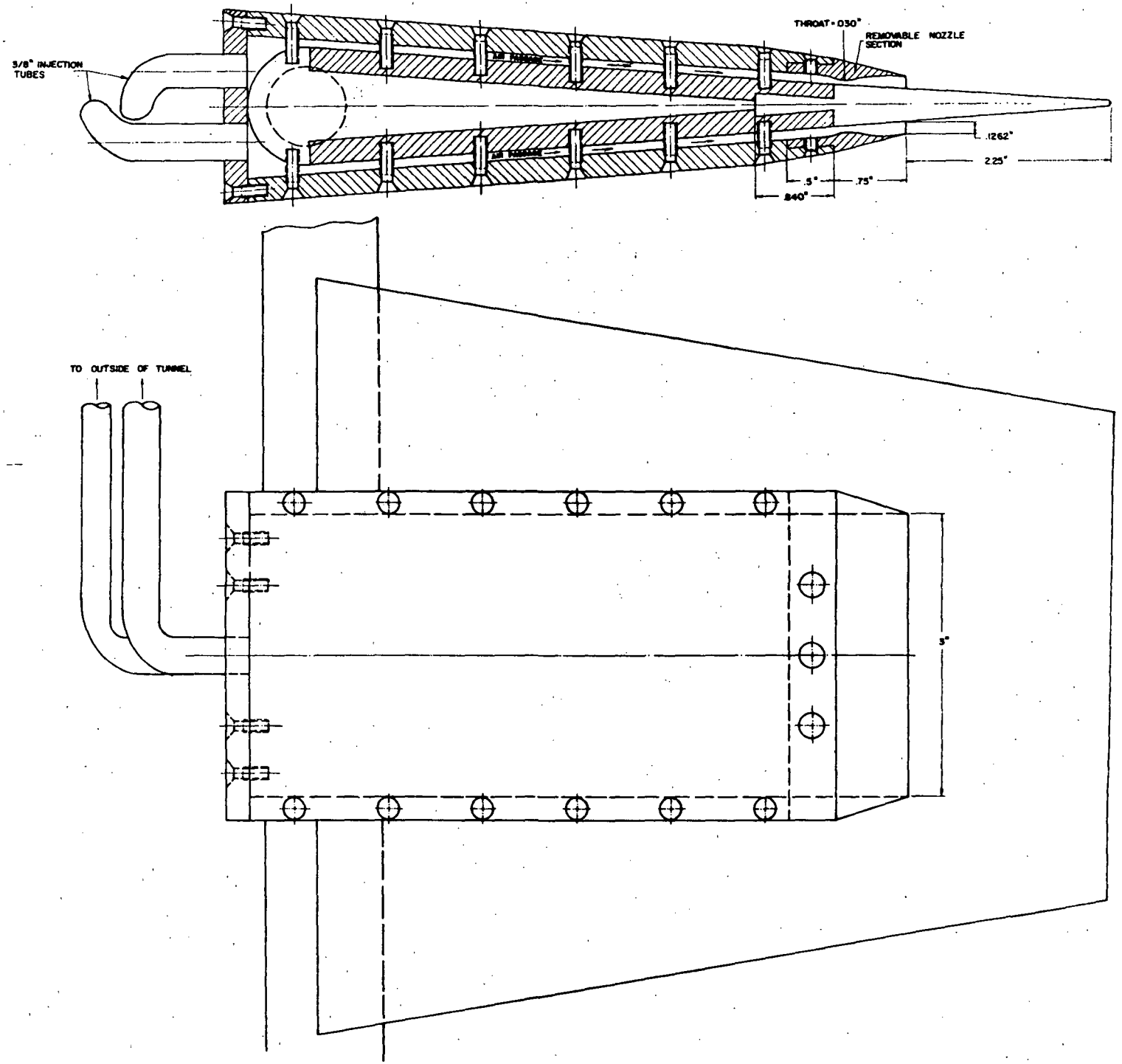
3/8" INJECTION TUBES
THROAT = .030"
REMOVABLE NOZZLE SECTION
.1262"
2.25"
.5"
.75"
.840"
TO OUTSIDE OF TUNNEL
3"

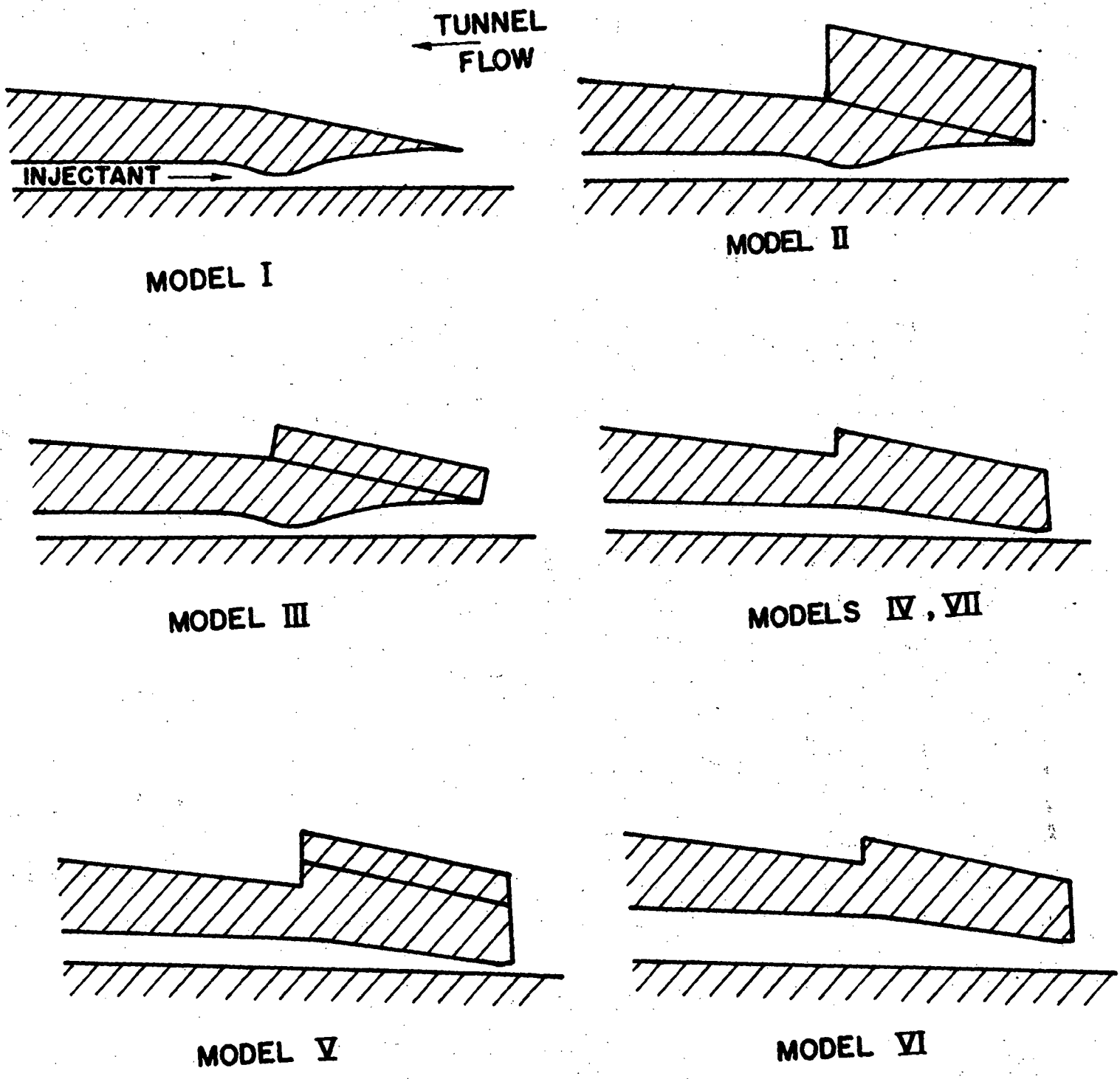

Fig. 8 Step and slot configurations investigated

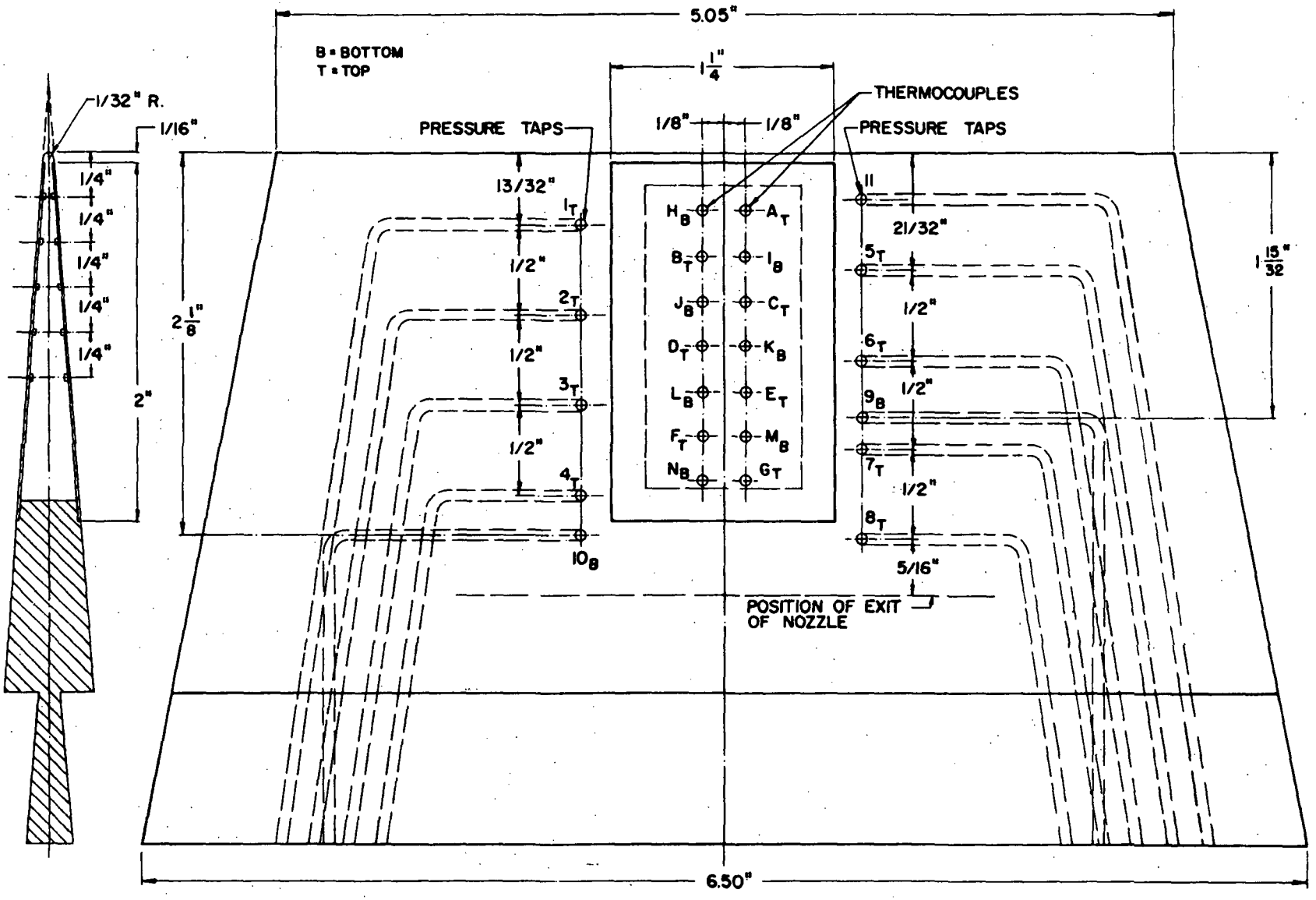

Fig. 9 Model instrumentation locations

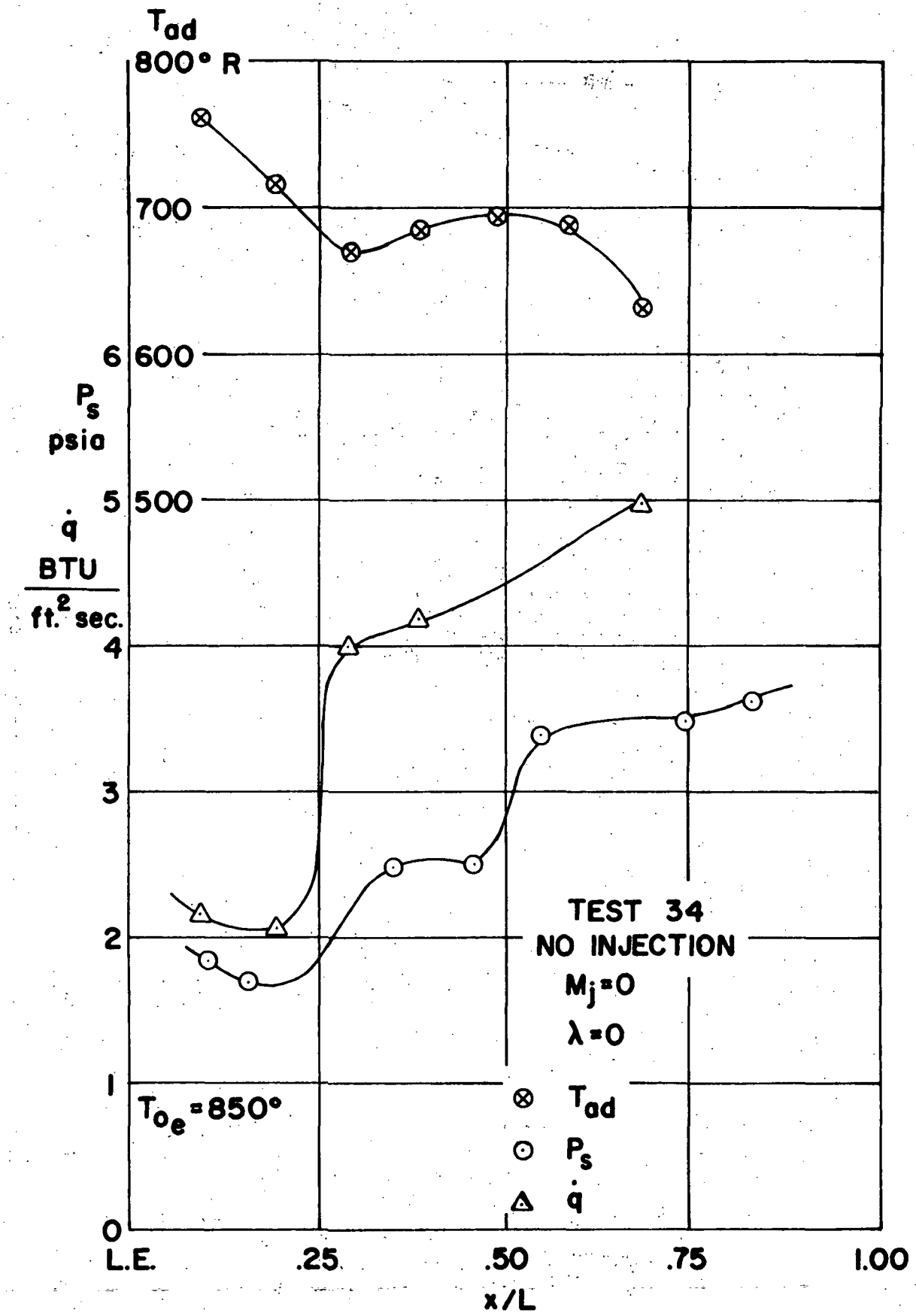

Fig. 10 Distributions of measured quantities along the wall between the leading edge and the injection slot

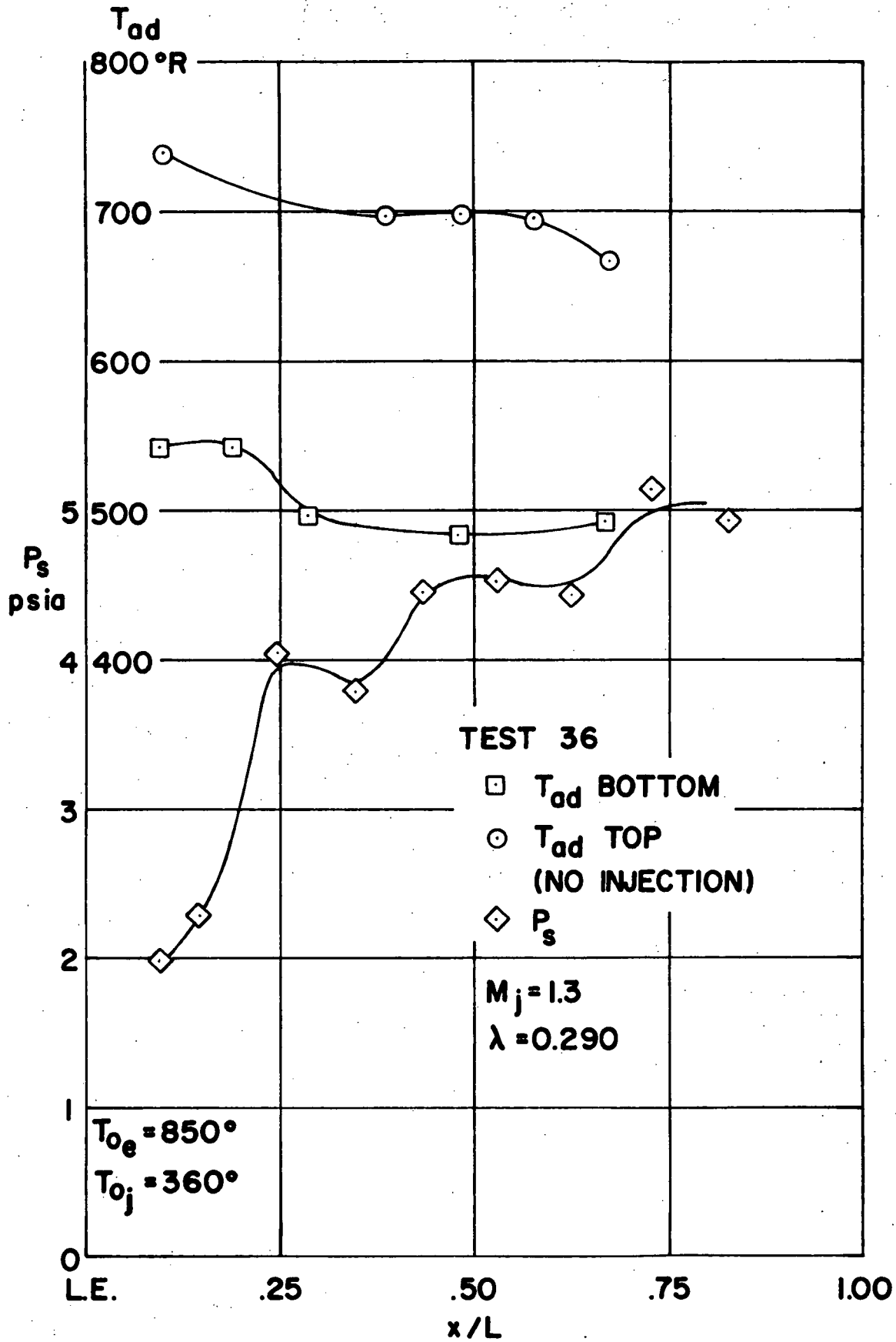

Fig. 11 Distributions of measured quantities along the wall between the leading edge and the injection slot

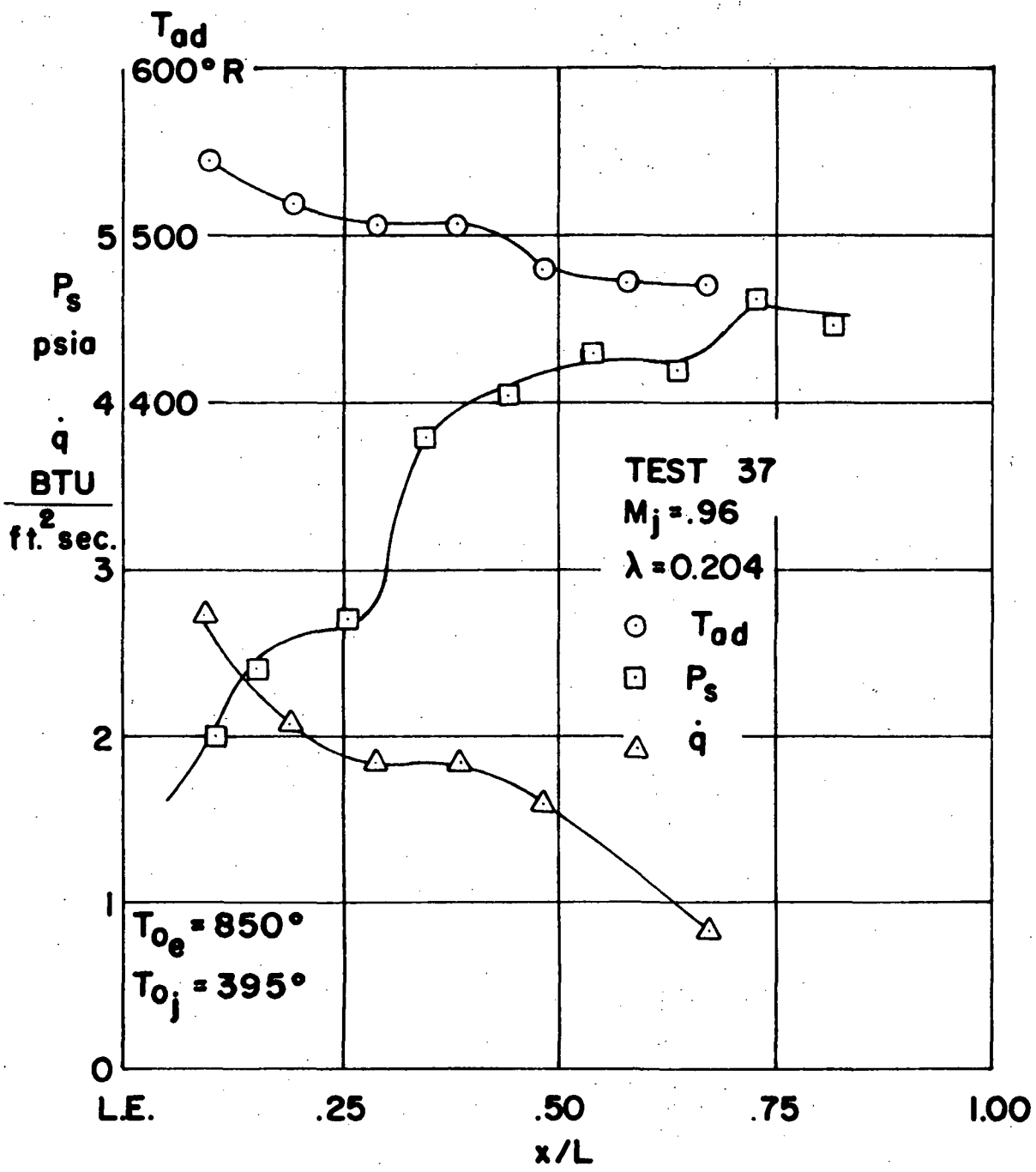

Fig. 12 Distributions of measured quantities along the wall between the leading edge and the injection slot

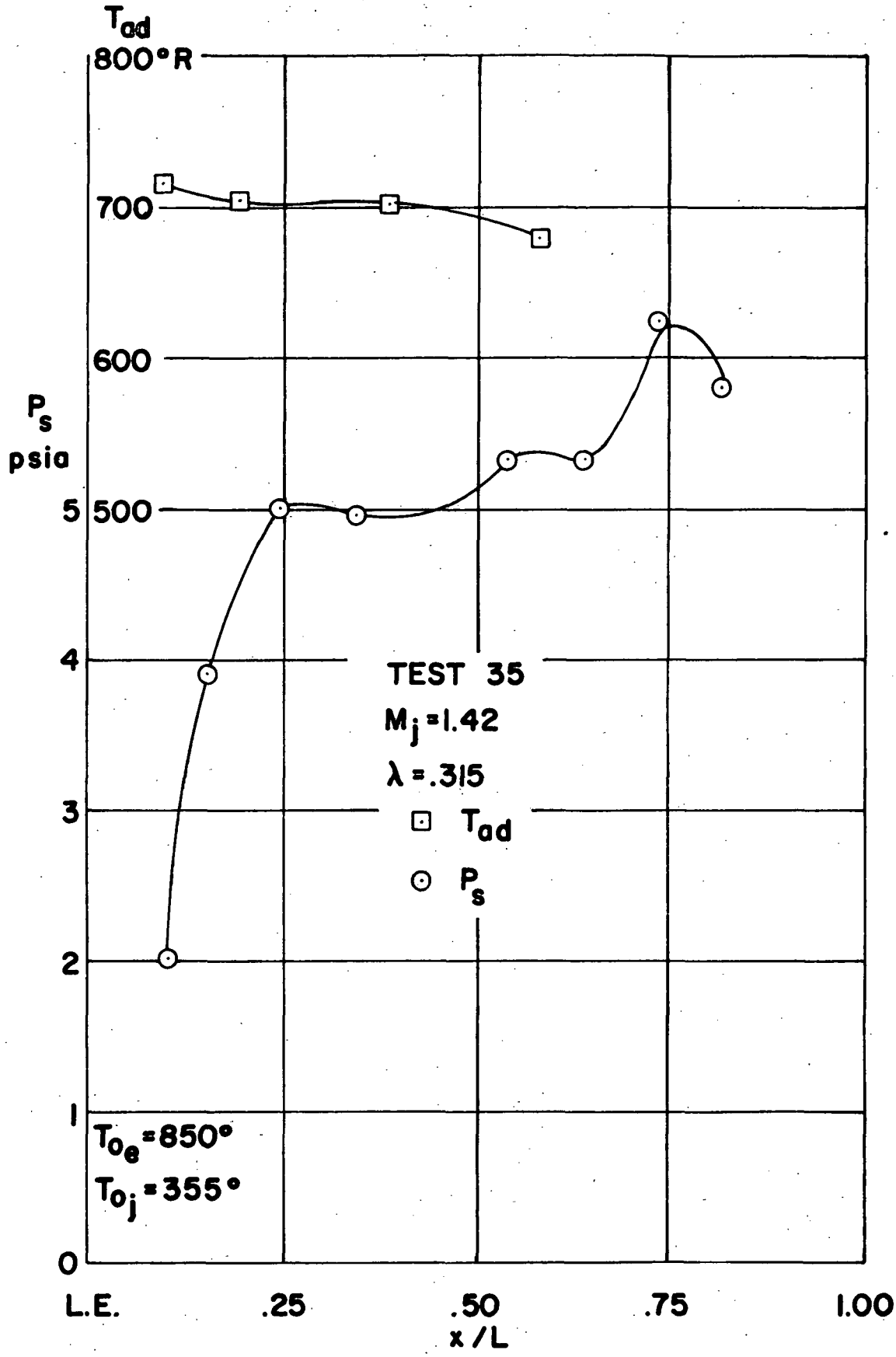

Fig. 13 Distributions of measured quantities along the wall between the leading edge and the injection slot

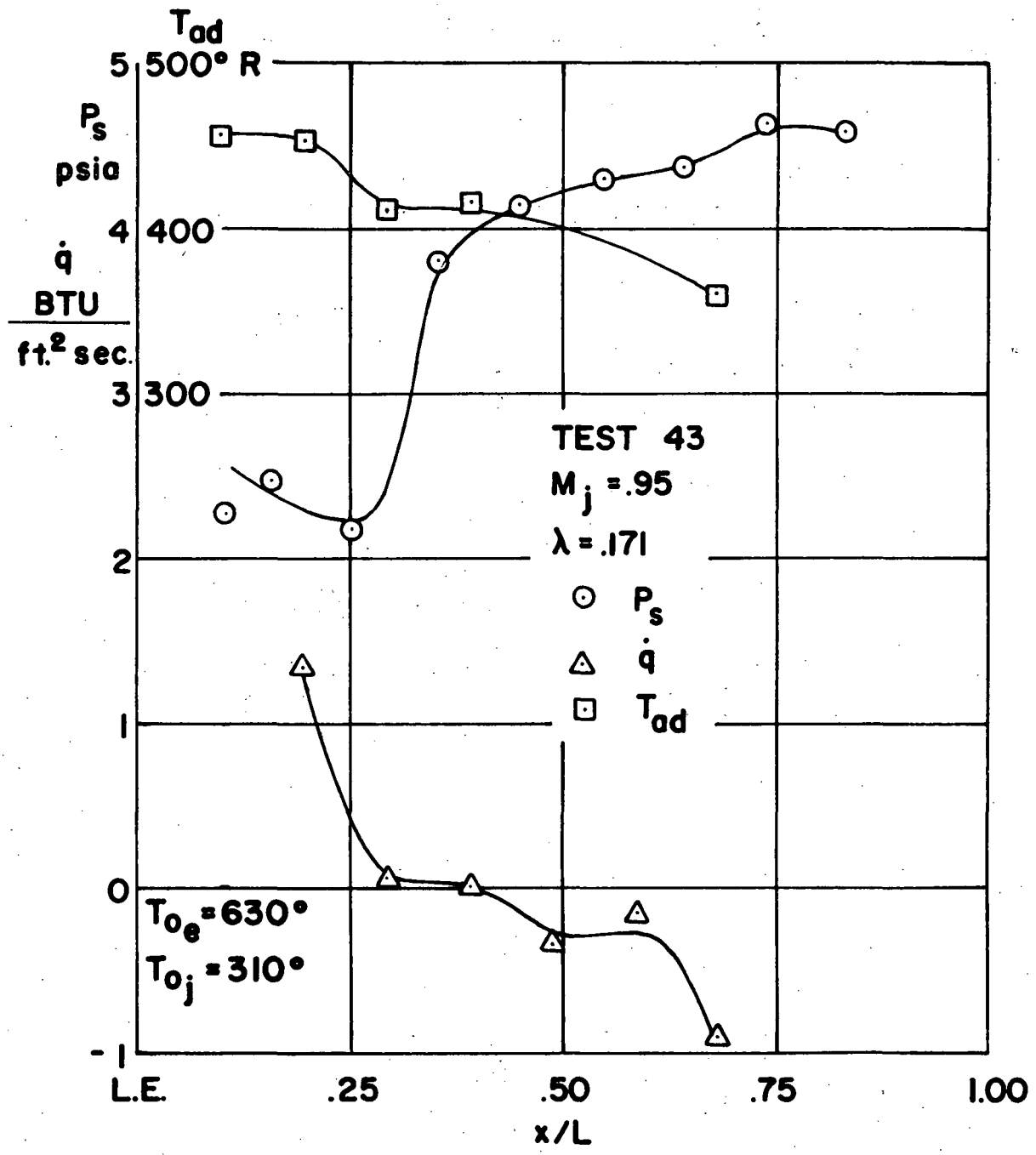

Fig. 14 Distributions of measured quantities along the wall between the leading edge and the injection slot

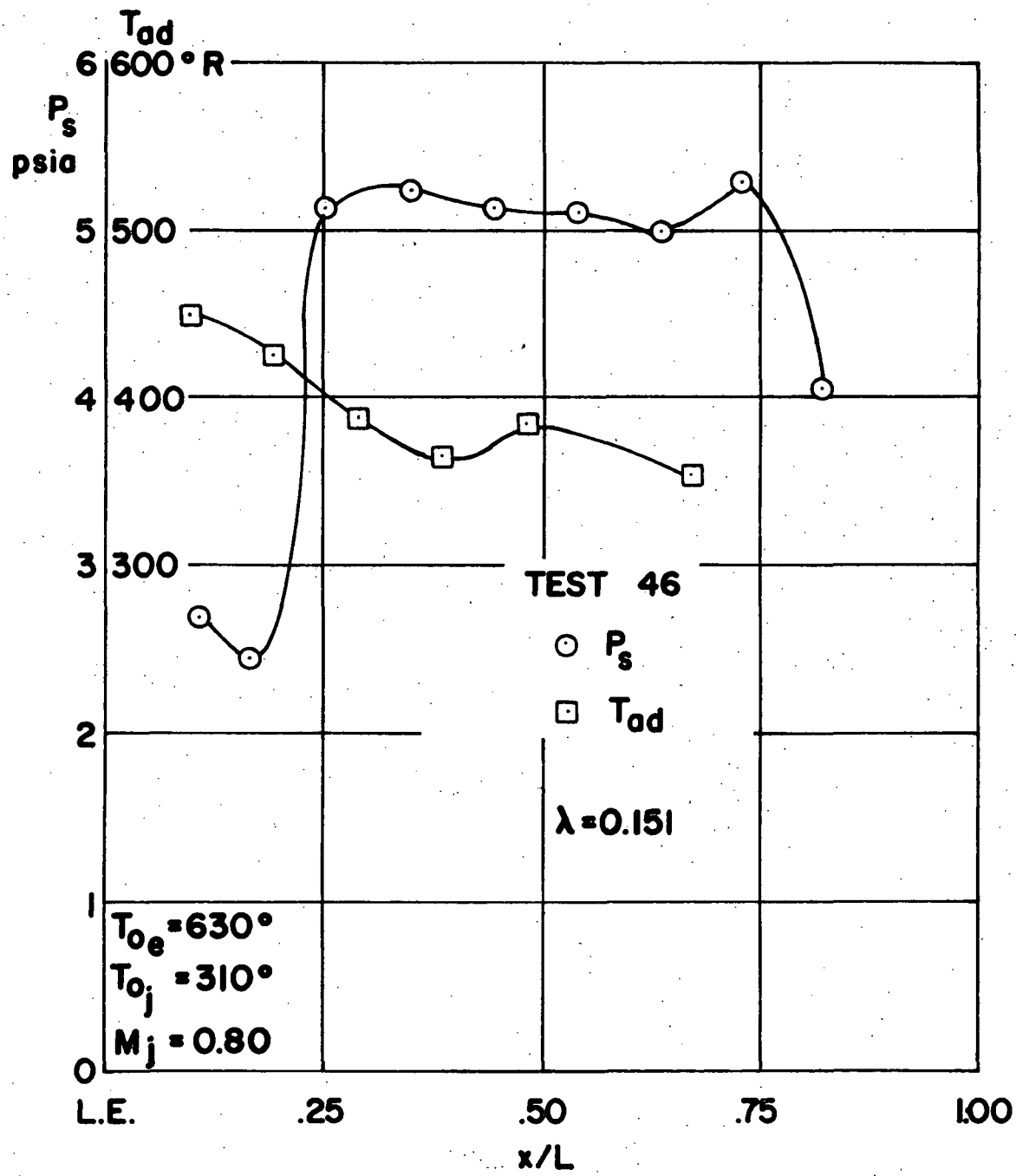

Fig. 15 Distributions of measured quantities along the wall between the leading edge and the injection slot

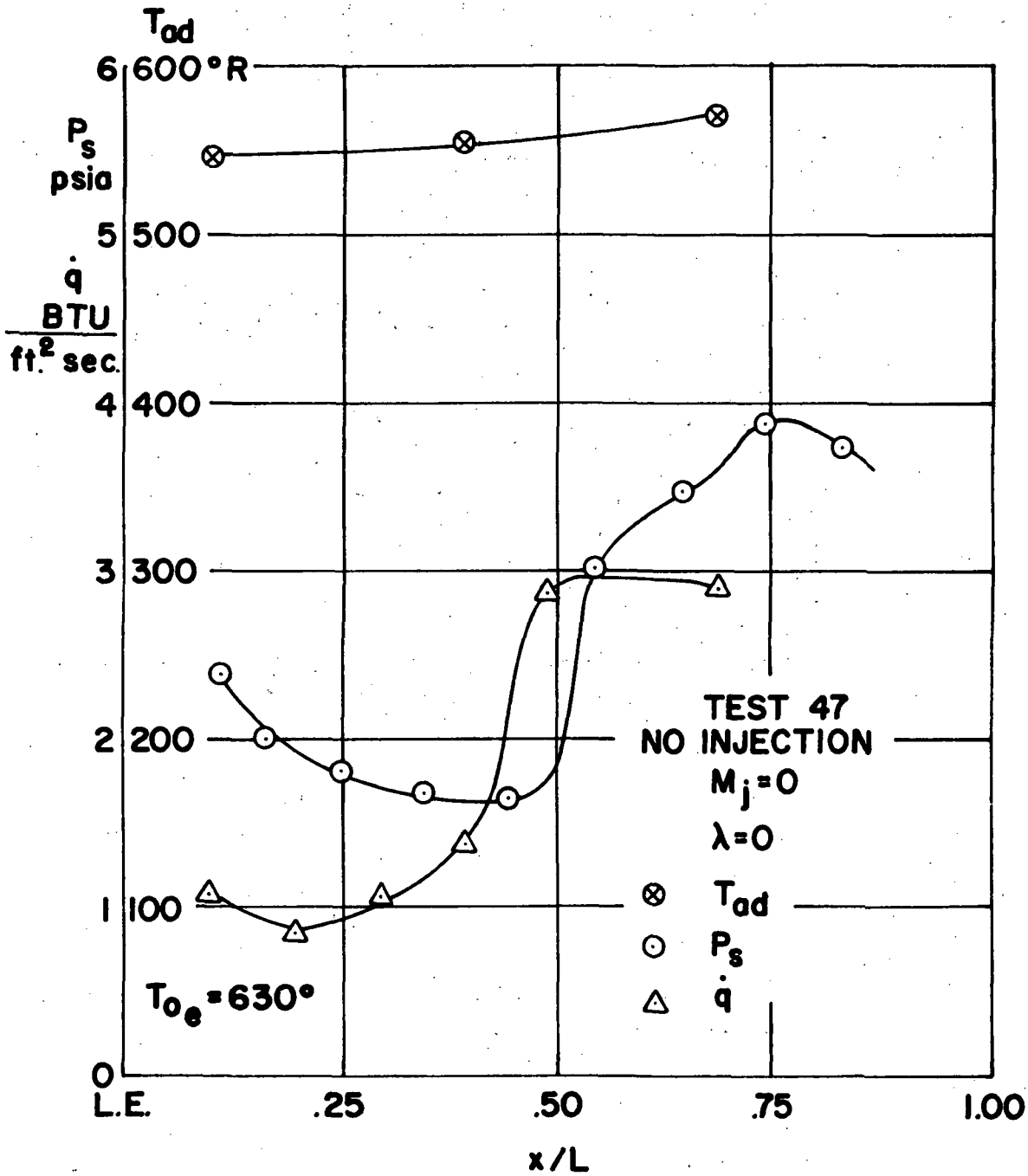

Fig. 16 Distributions of measured quantities along the wall between the leading edge and the injection slot

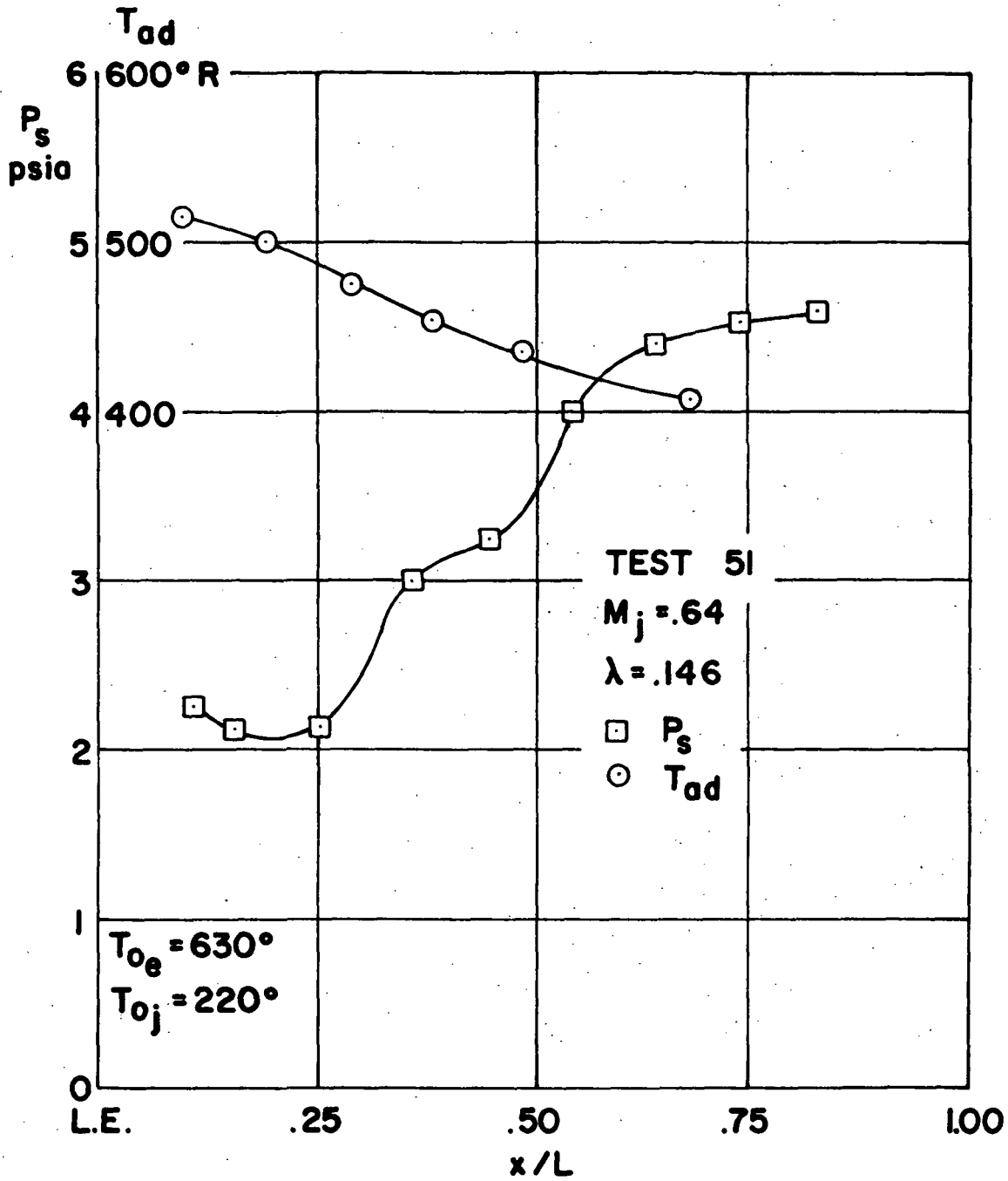

Fig. 17 Distributions of measured quantities along the wall between the leading edge and the injection slot

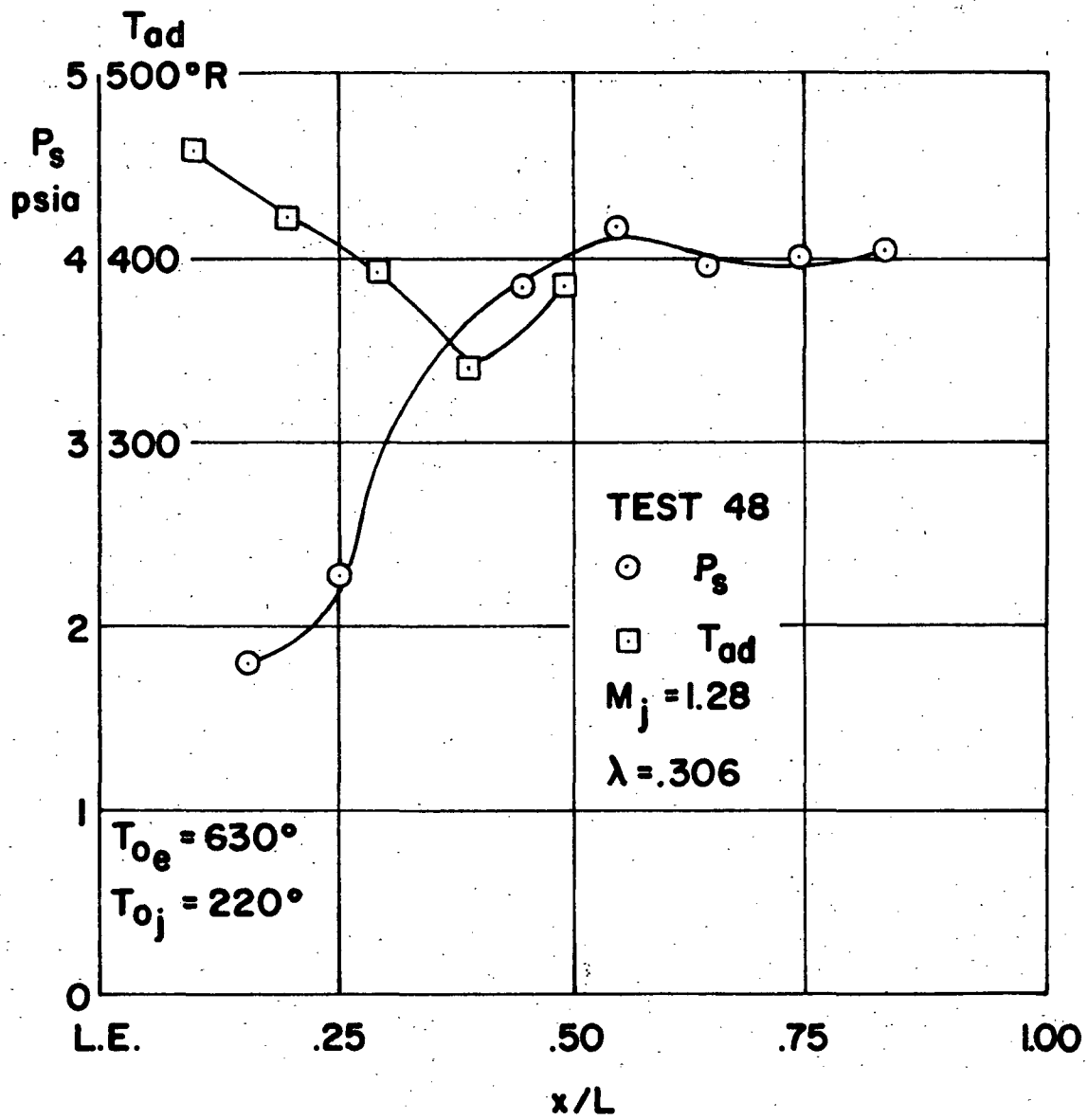

Fig. 18 Distributions of measured quantities along the wall between the leading edge and the injection slot

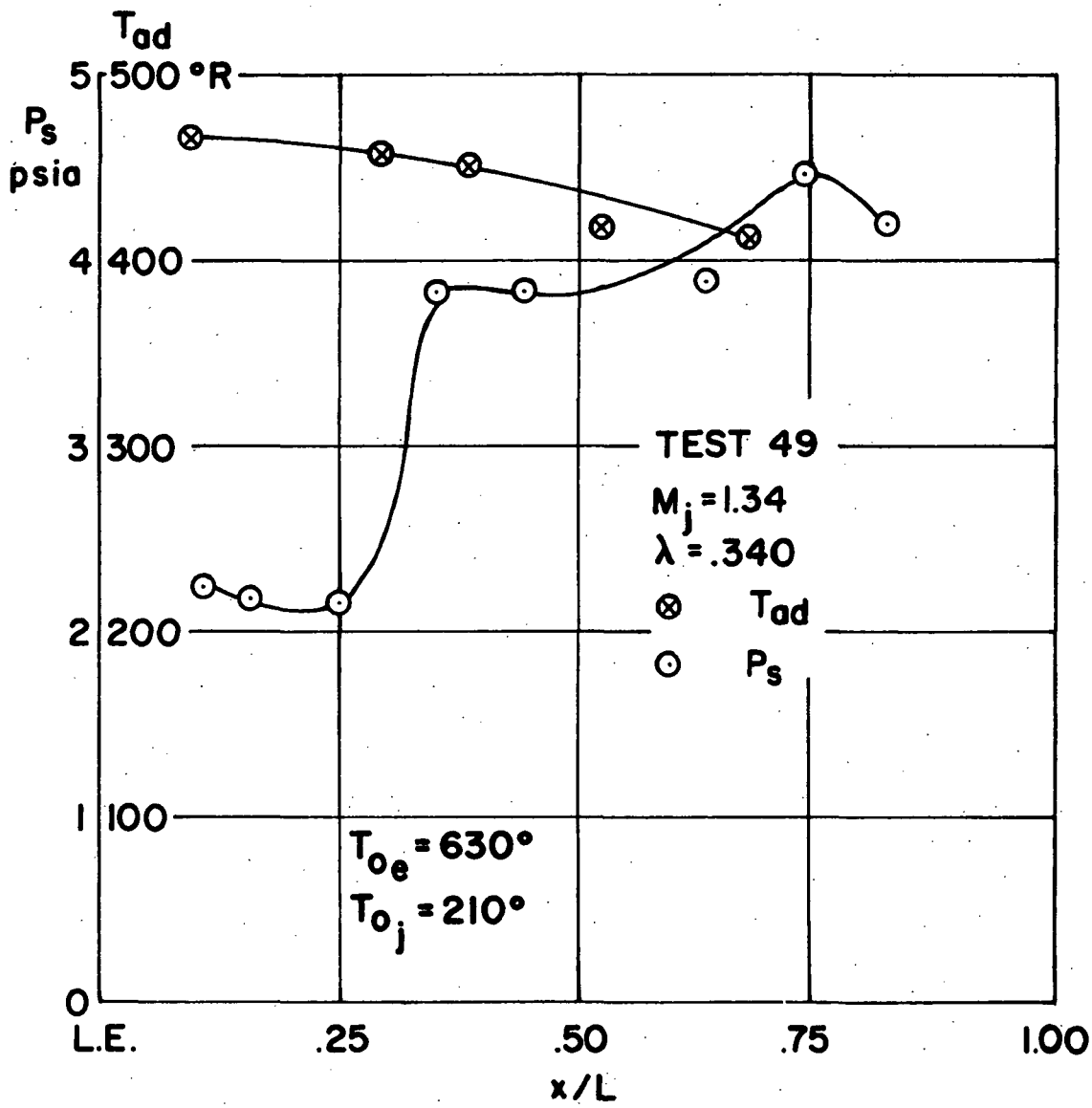

Fig. 19 Distributions of measured quantities along the wall between the leading edge and the injection slot

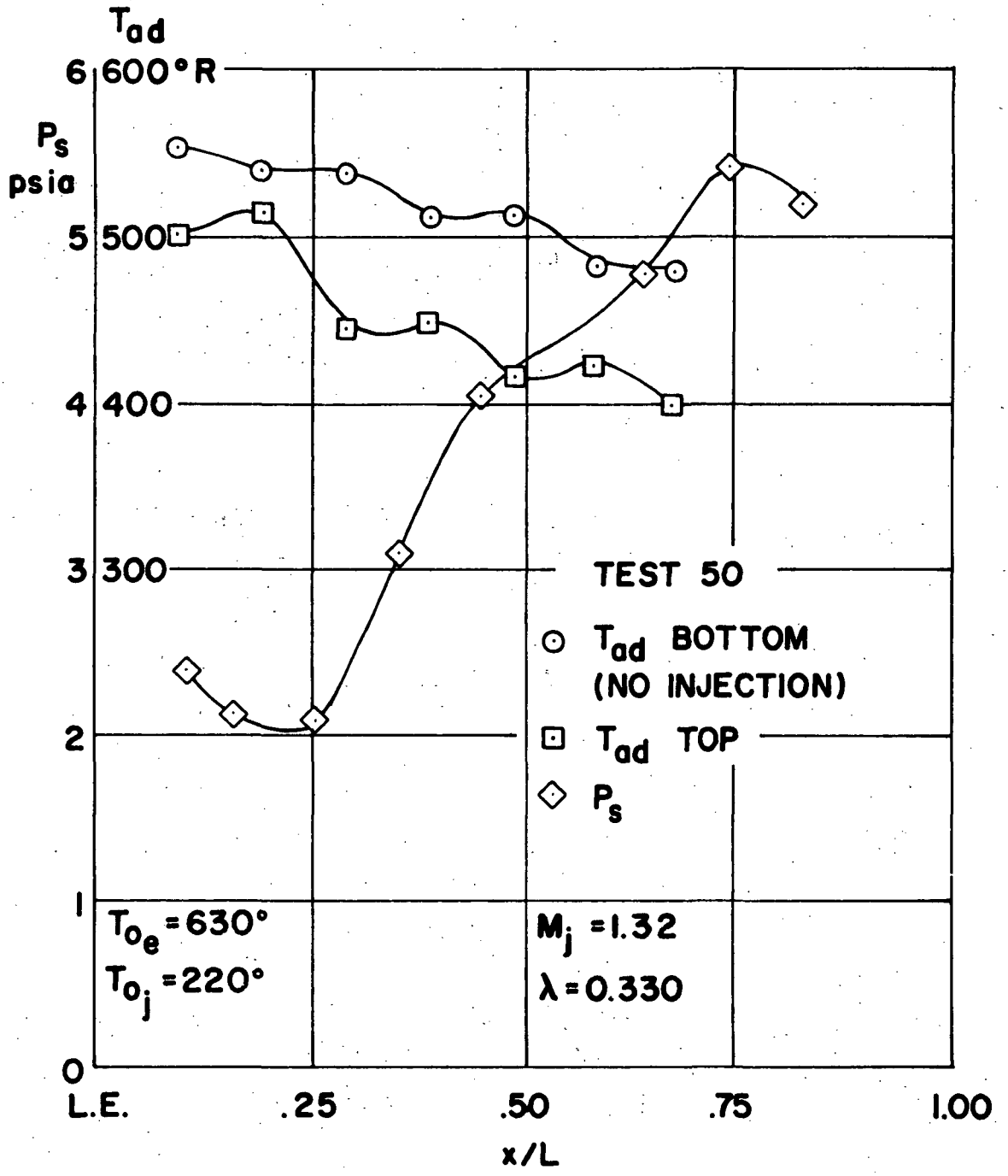

Fig. 20 Distributions of measured quantities along the wall between the leading edge and the injection slot

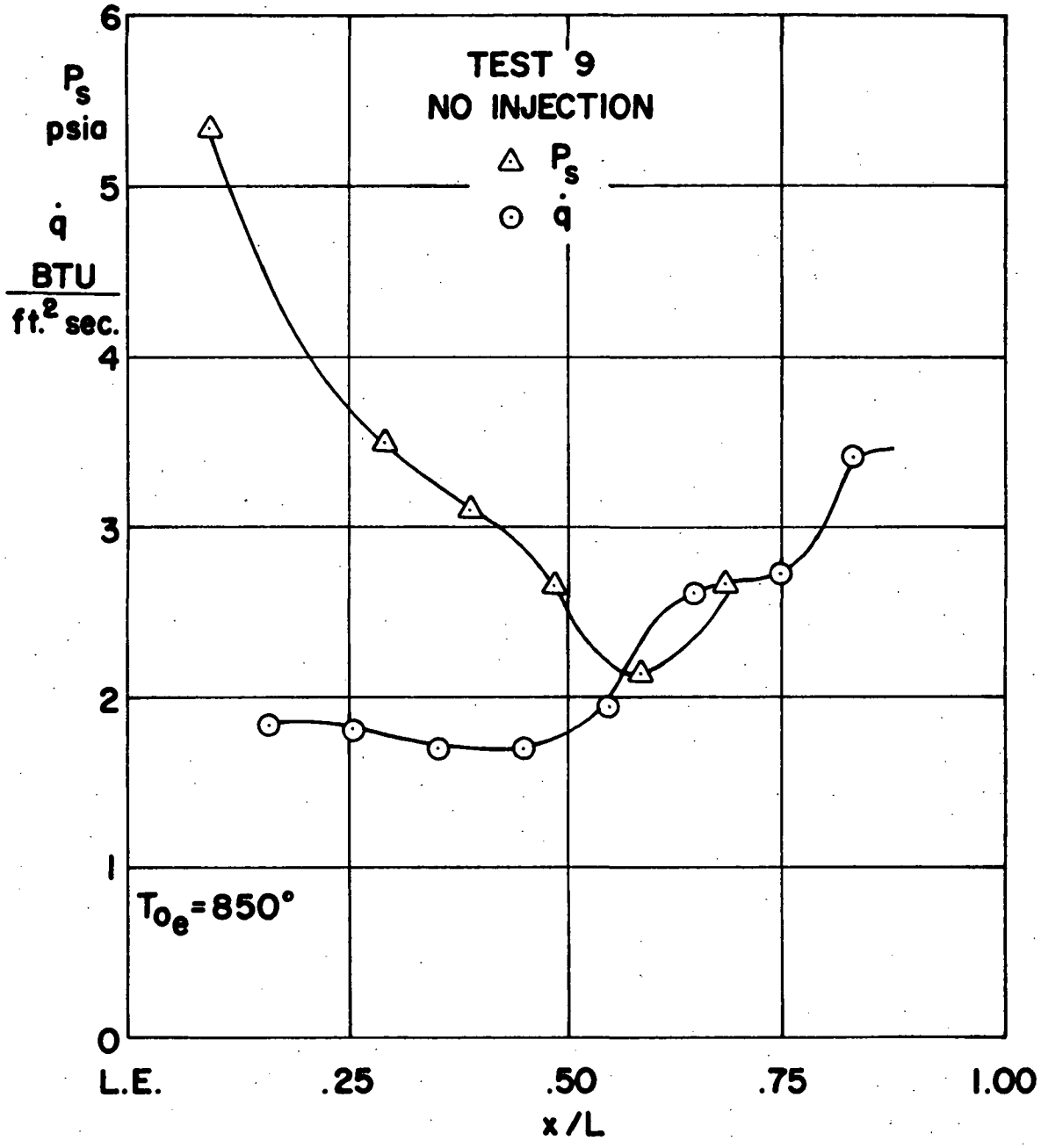

Fig. 21 Distributions of measured quantities along the wall between the leading edge and the injection slot

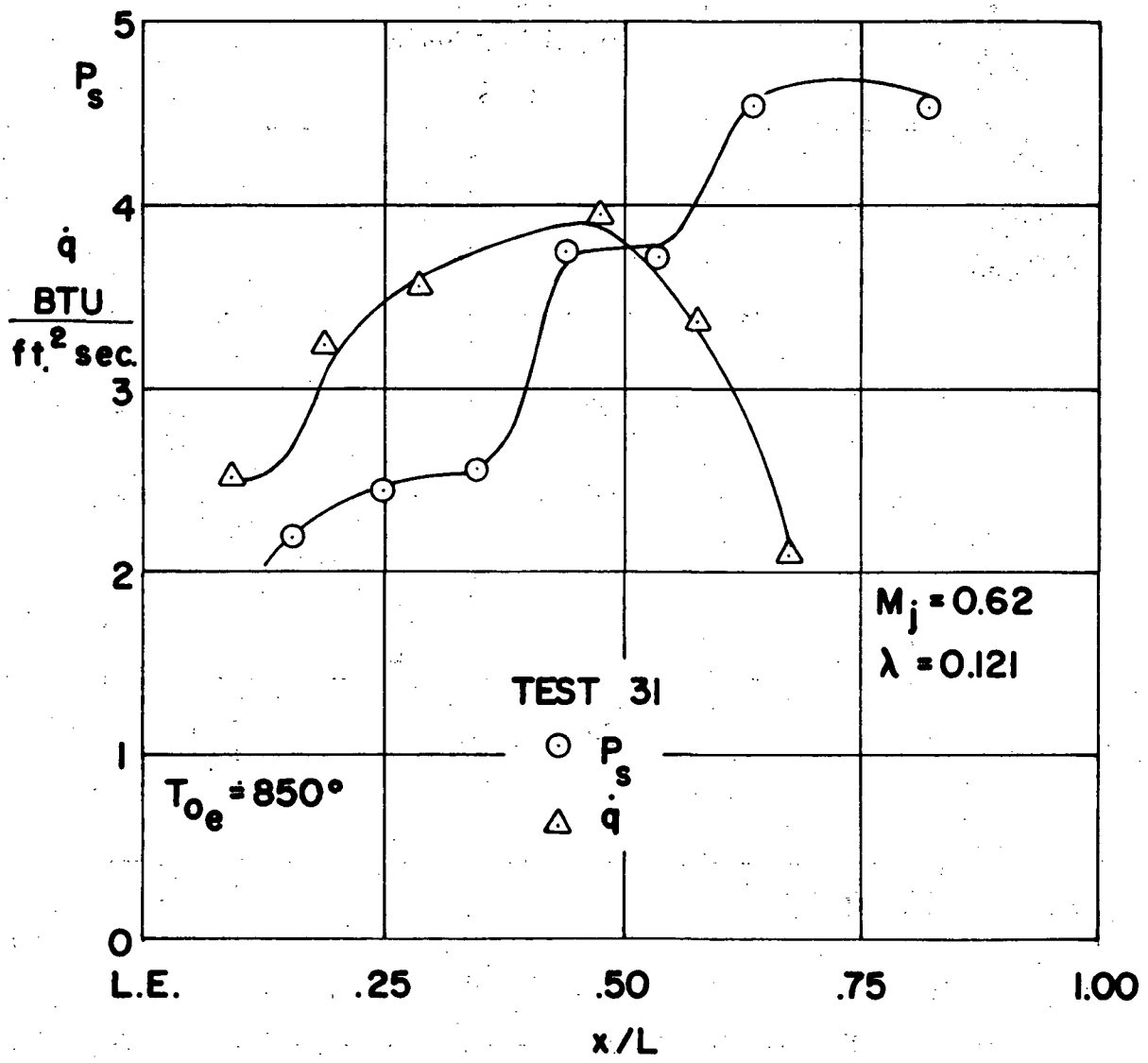

Fig. 22 Distributions of measured quantities along the wall between the leading edge and the injection slot

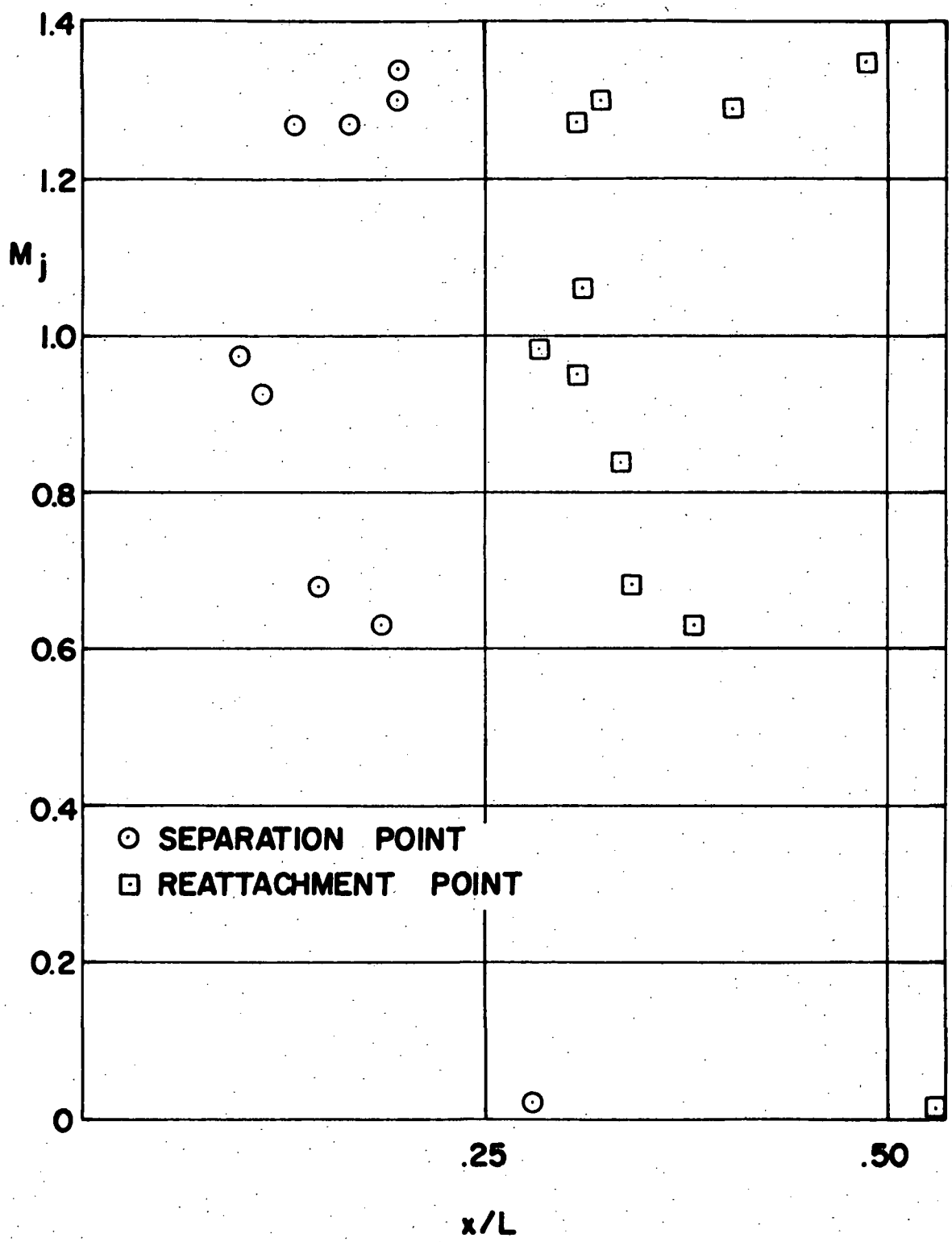

Fig. 23 Separation and reattachment points as a function of jet Mach number

MODEL	TESTS	S/ℓ	ℓ/L	S	ℓ	ℓ_p
I	1-17	1.00	0.0496	.127	.127	0
II	18-25,29	.328	0.152	.127	.388	.261
III	26-28	.526	0.094	.127	.241	.114
IV	30-32	.149	0.092	.035	.235	.200
V	33	.100	0.137	.035	.349	.314
VI	34-46	.343	0.120	.105	.305	.200
VII	47-54	.152	0.092	.036	.236	.200
VI_B	46	.242	0.170	.105	.430	.325

Fig. 24 Table of geometrical parameters (*all dimensions in inches)

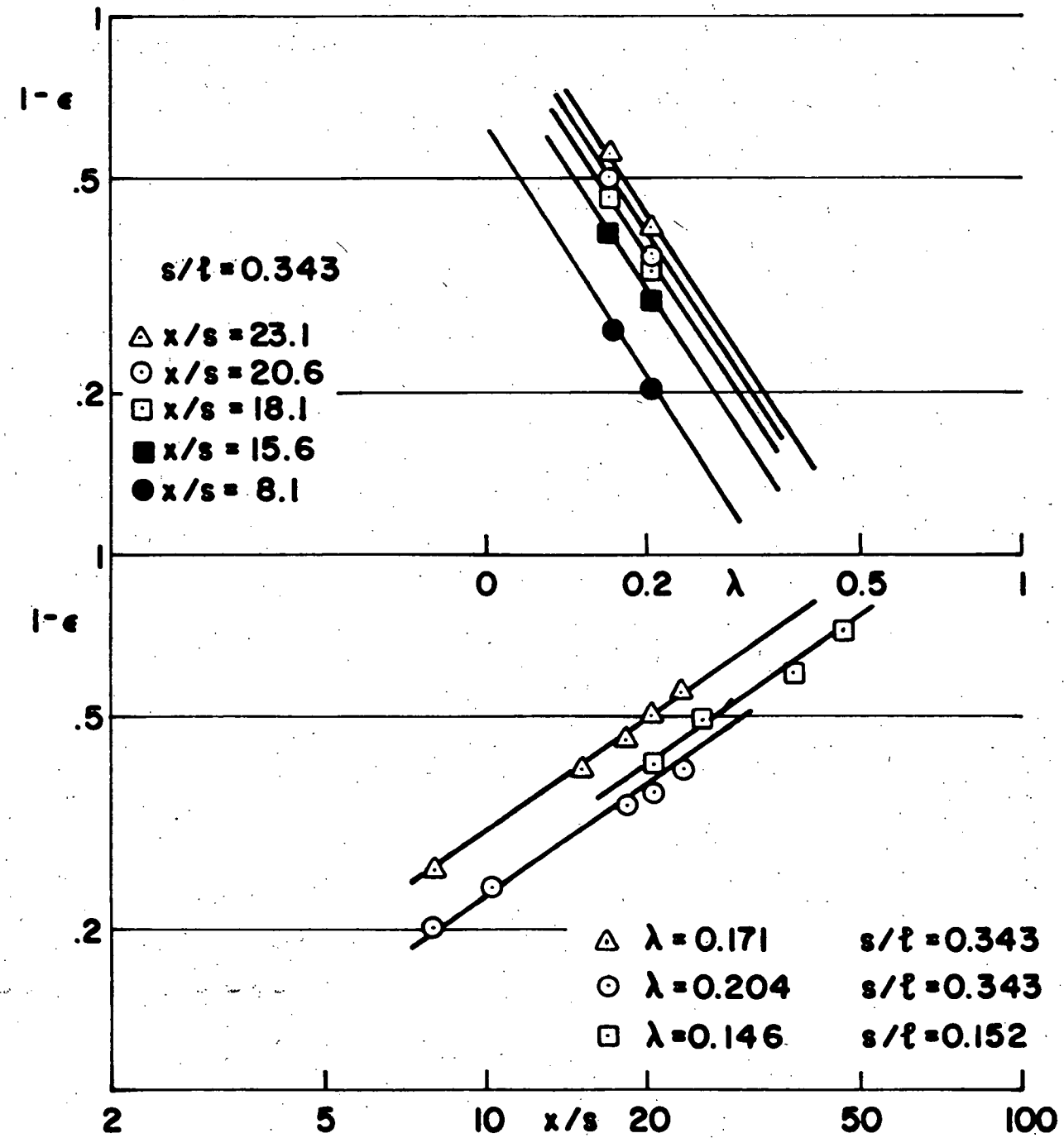

Fig. 25 Correlation of results

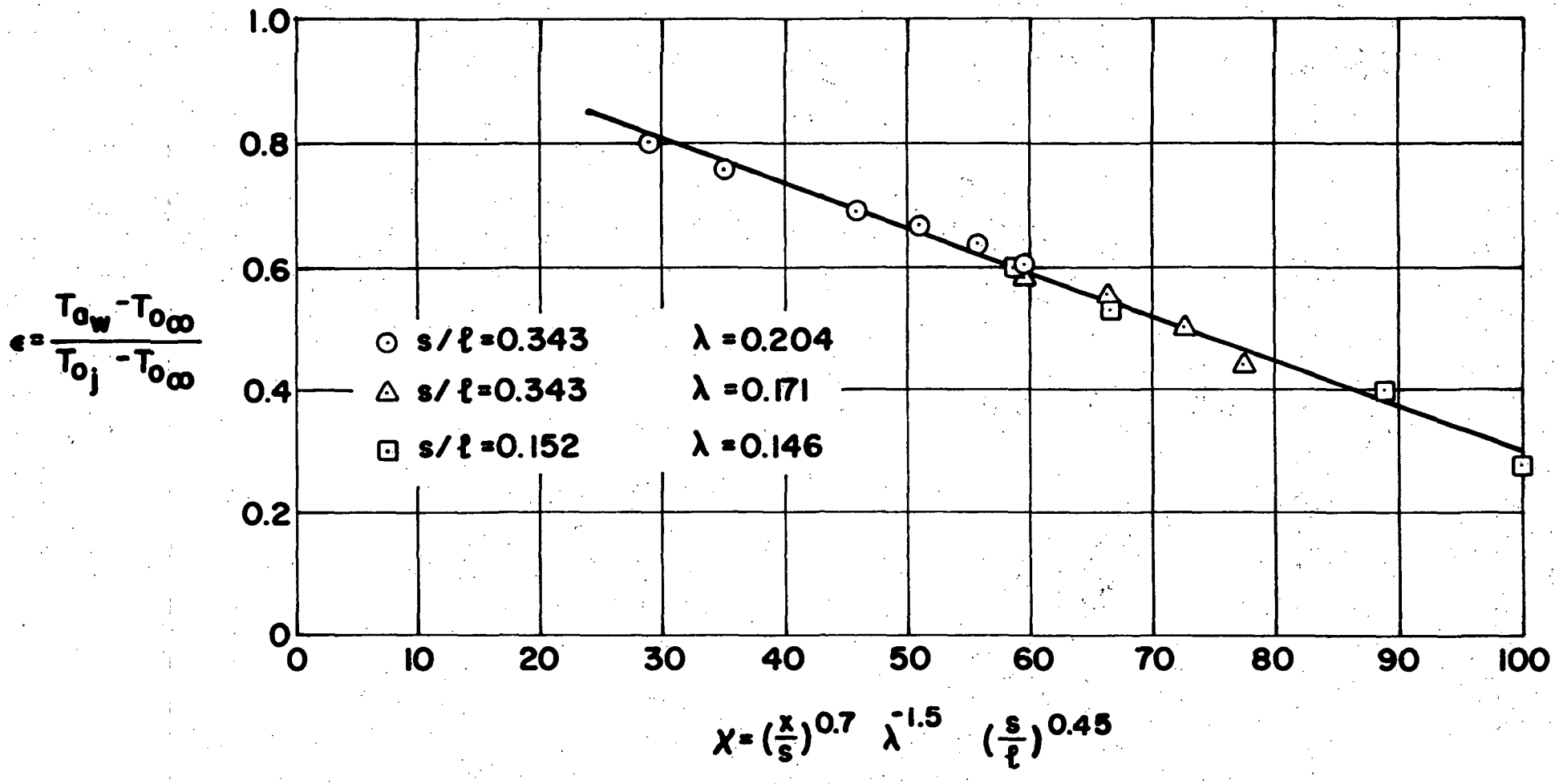

Fig. 26 Cooling effectiveness

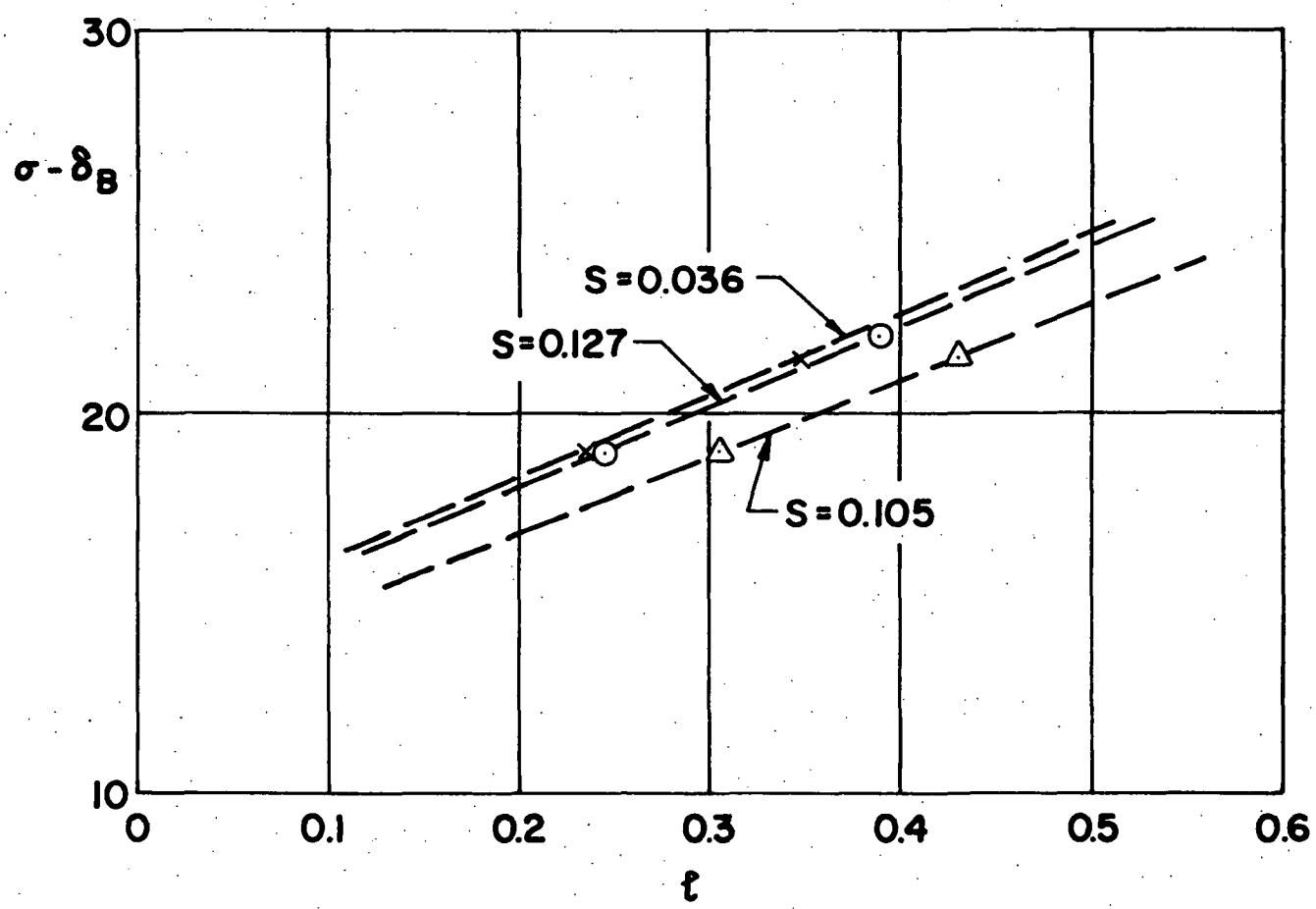

Fig. 27 Dividing streamline angle as a function of the step and slot heights

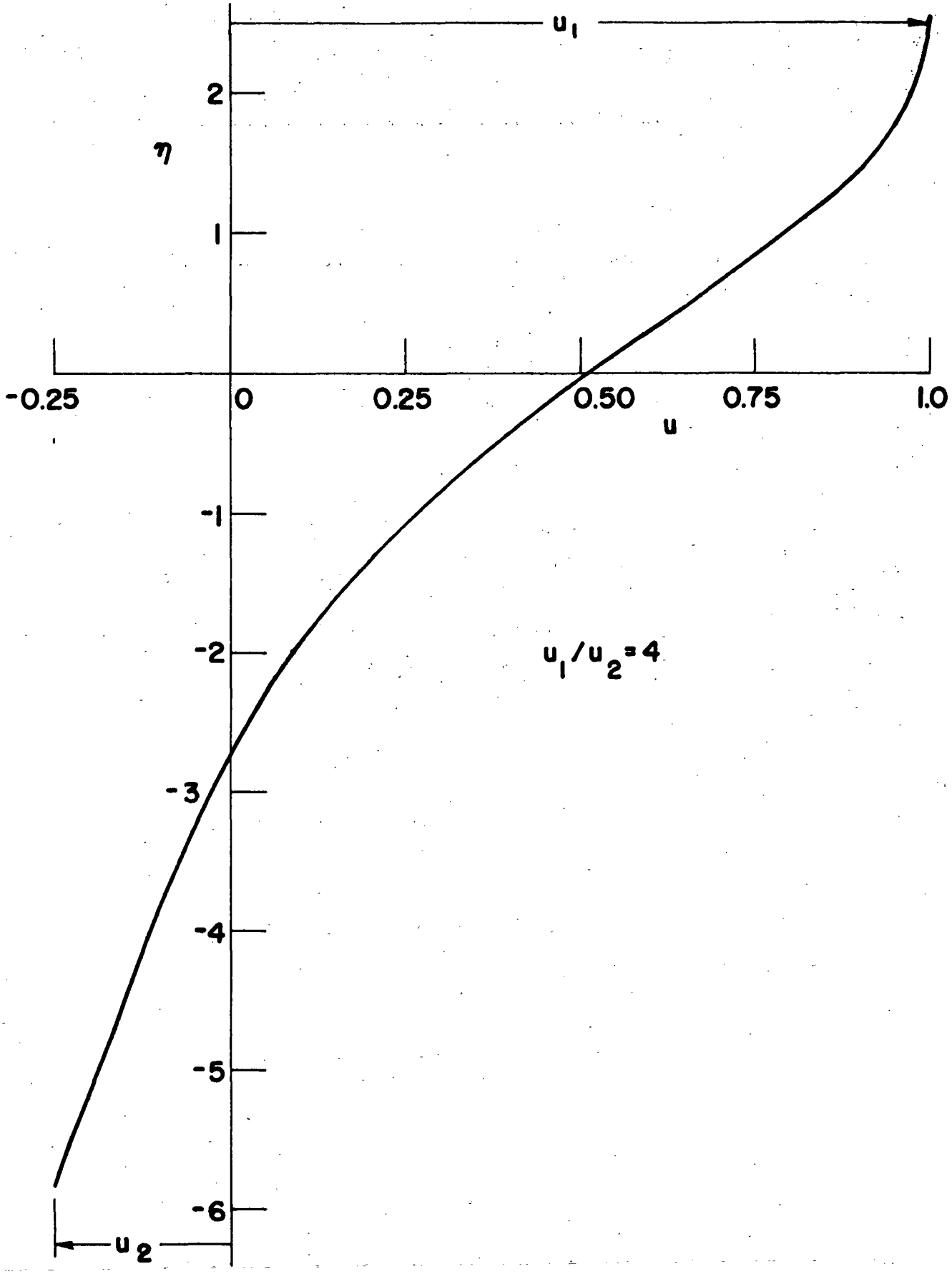

Fig. 28 Similar solution; nondimensional velocity profile

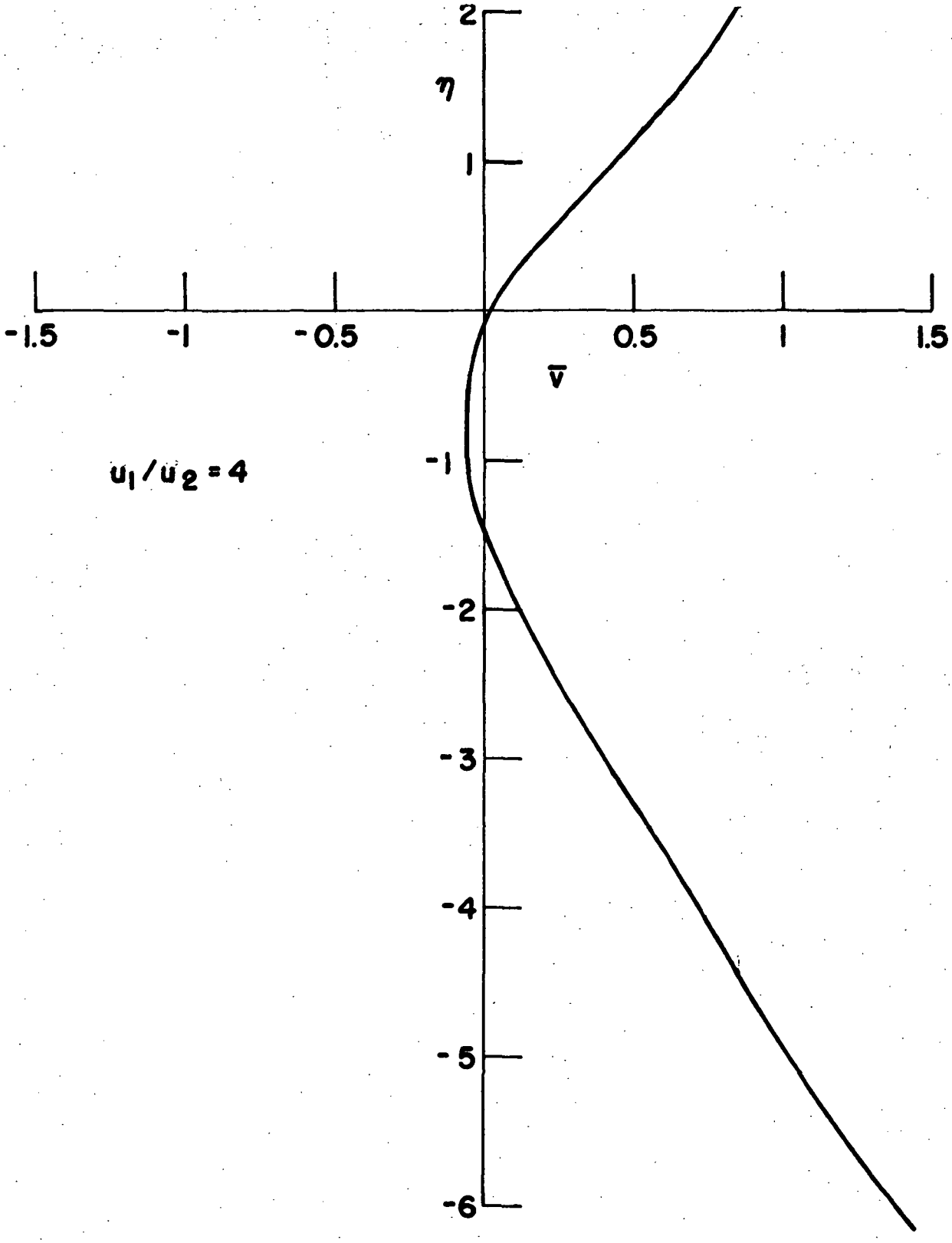

Fig. 29 Similar solution; nondimensional normal velocity profile

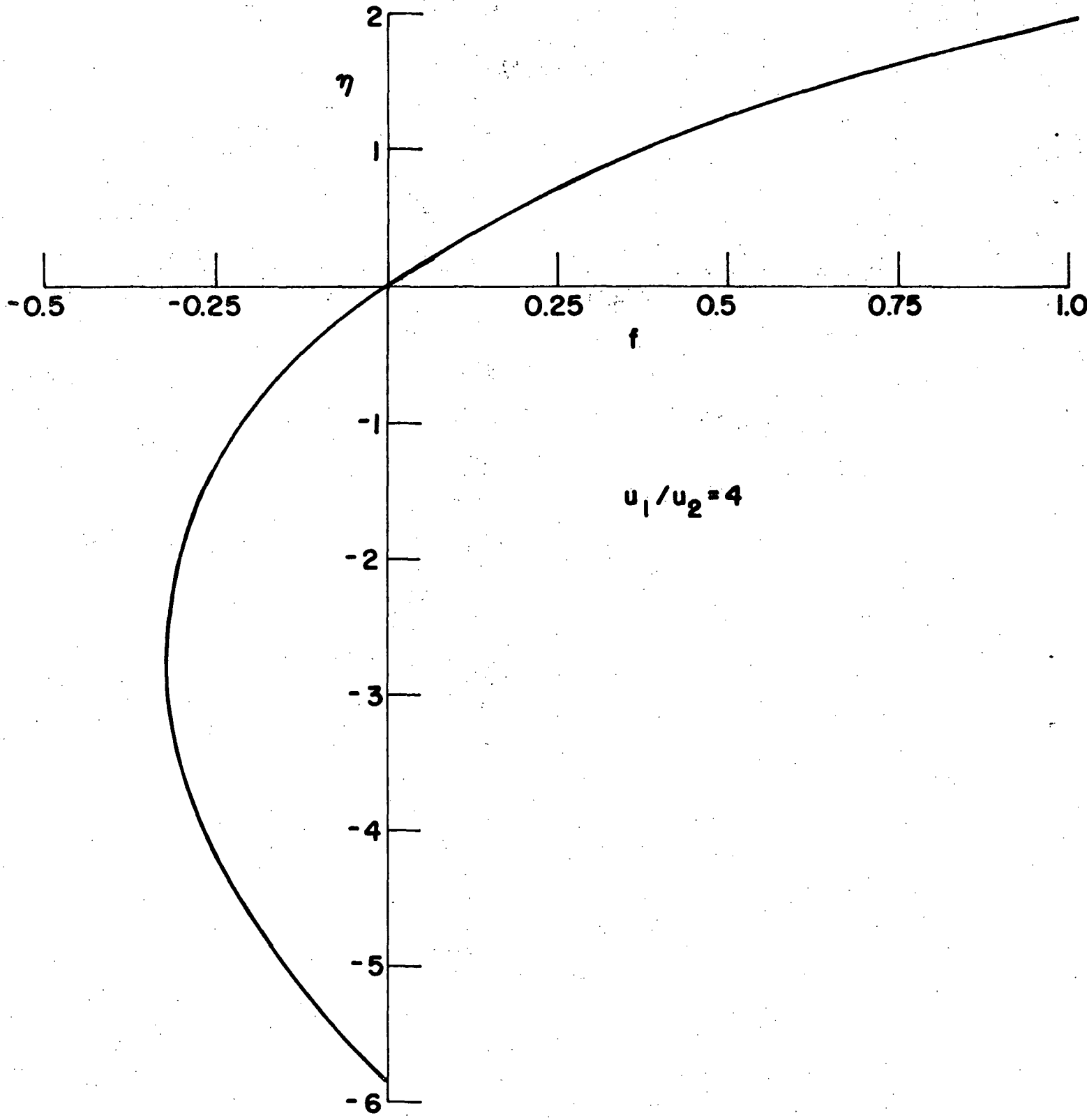

Fig. 30 Similar solution; nondimensional stream function profile

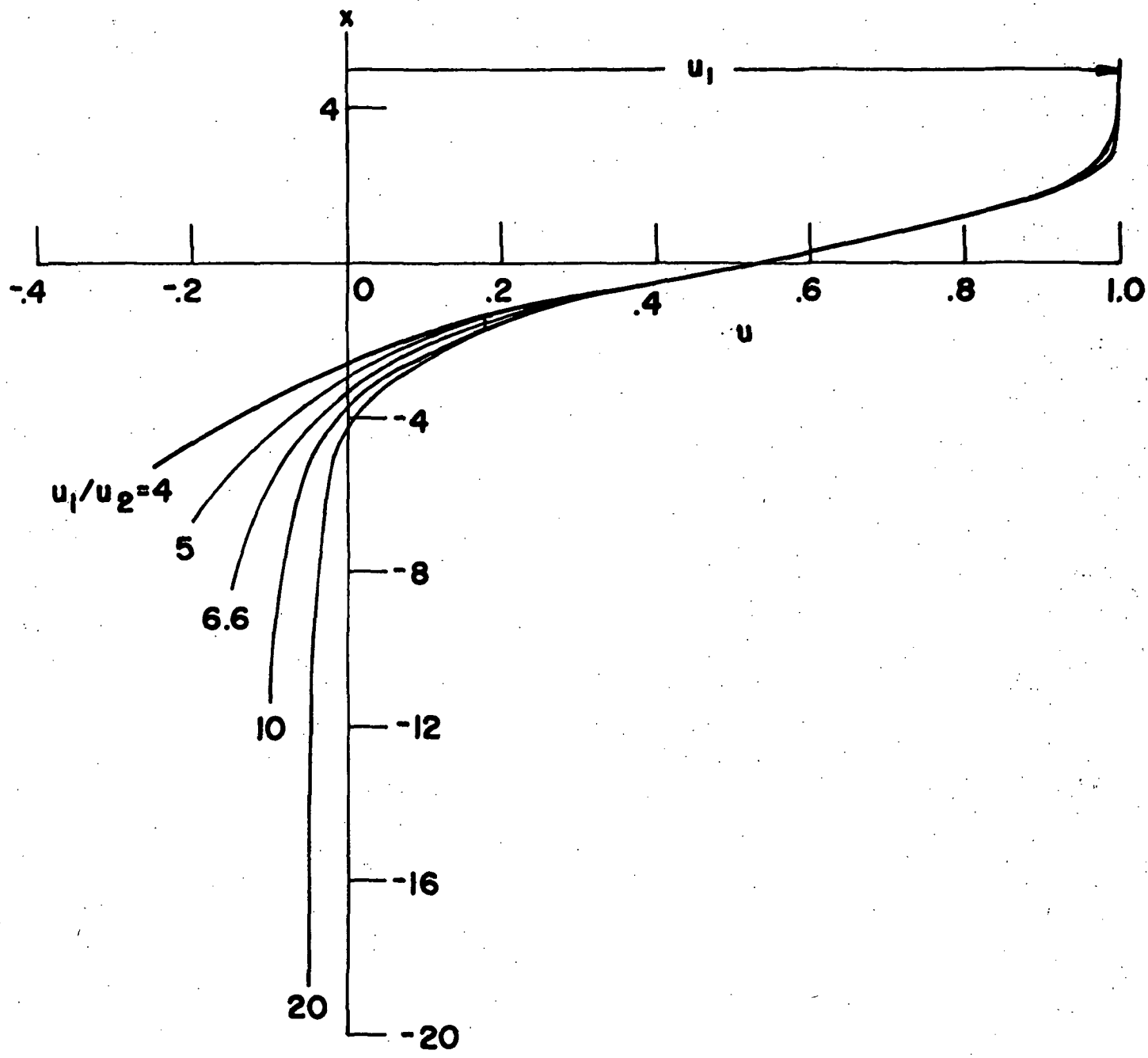

Fig. 31 Similar solution; nondimensional velocity profiles

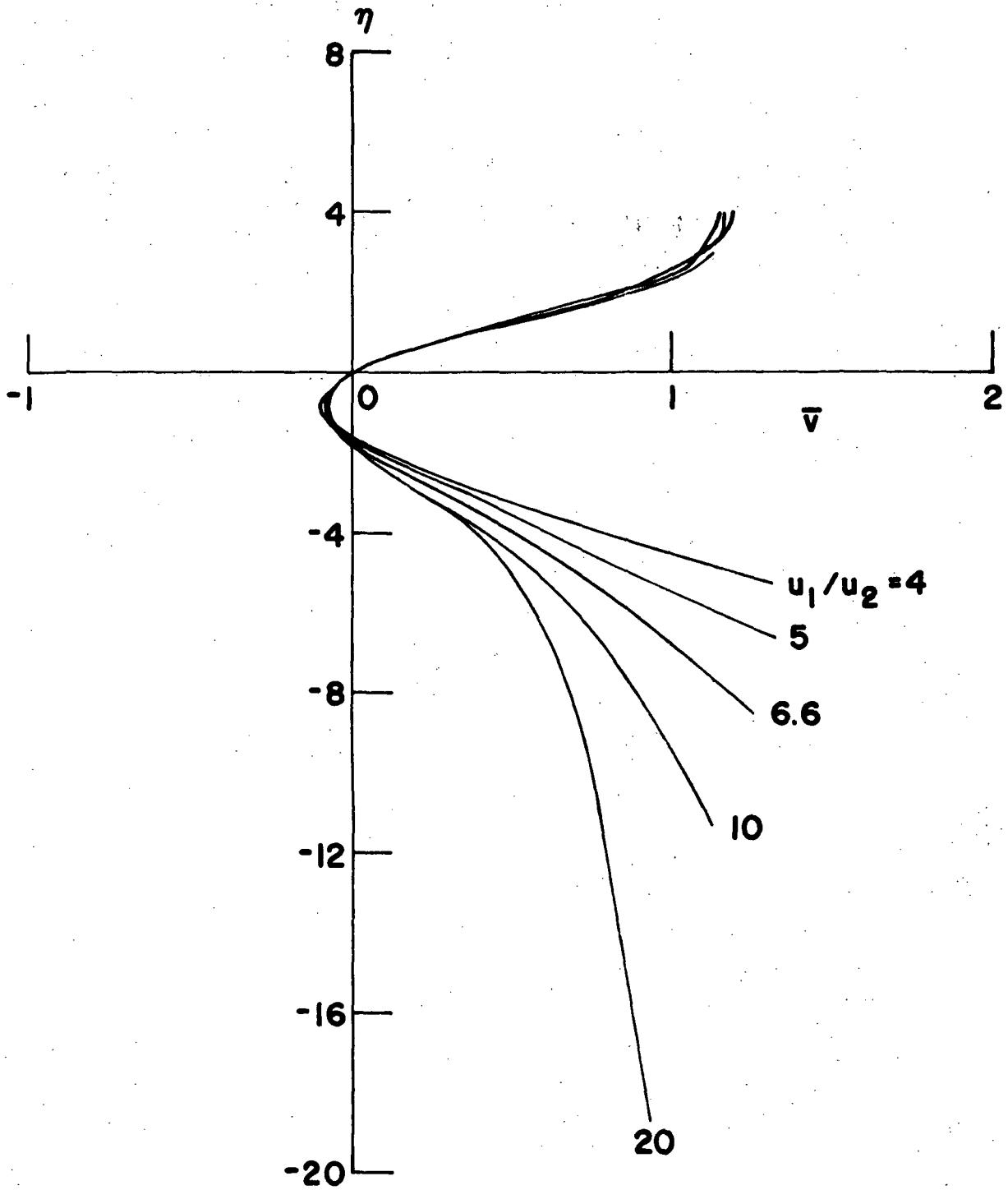

Fig. 32 Similar solution; nondimensional normal velocity profiles

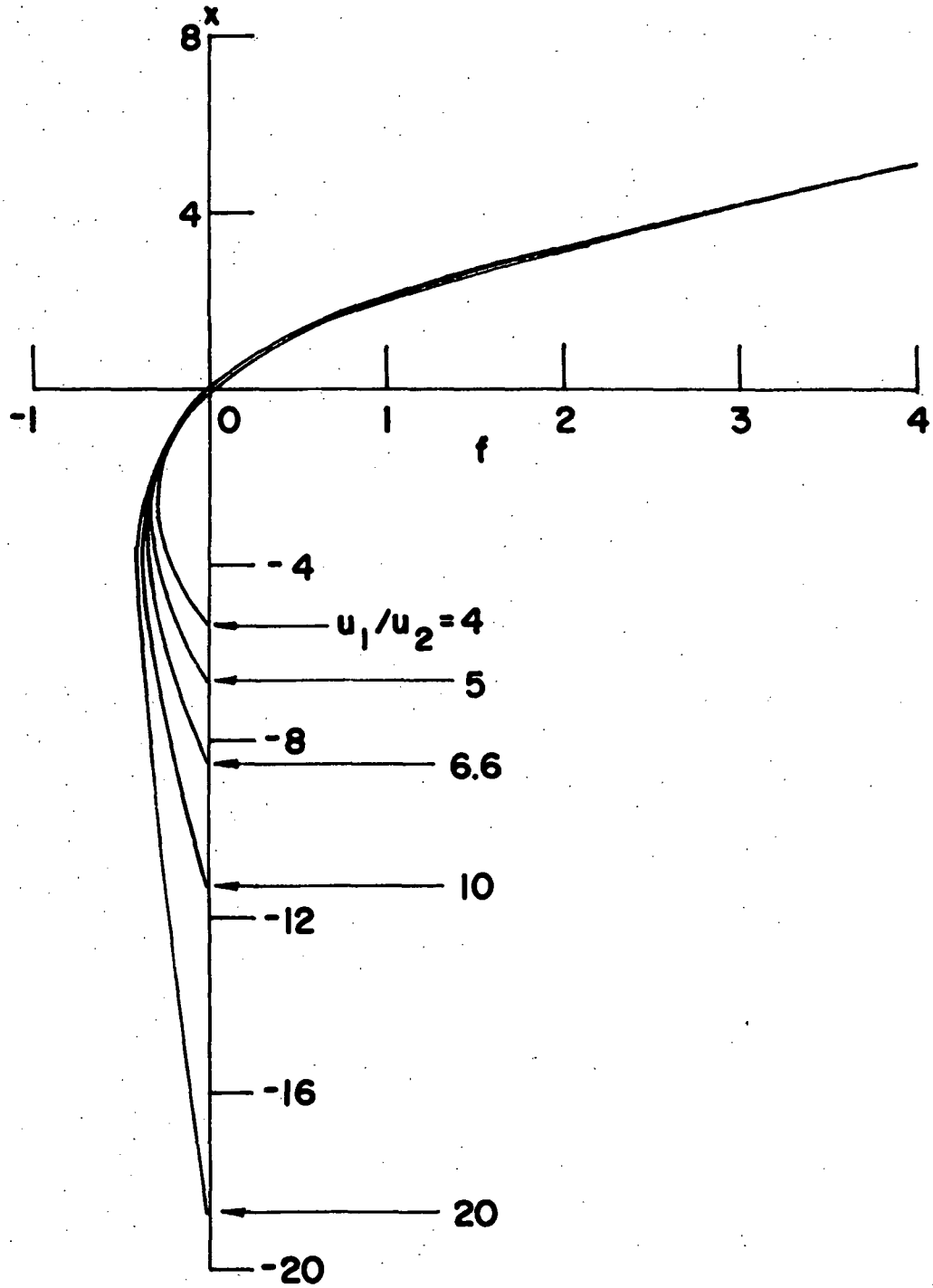

Fig. 33 Similar Solution; nondimensional stream function profiles

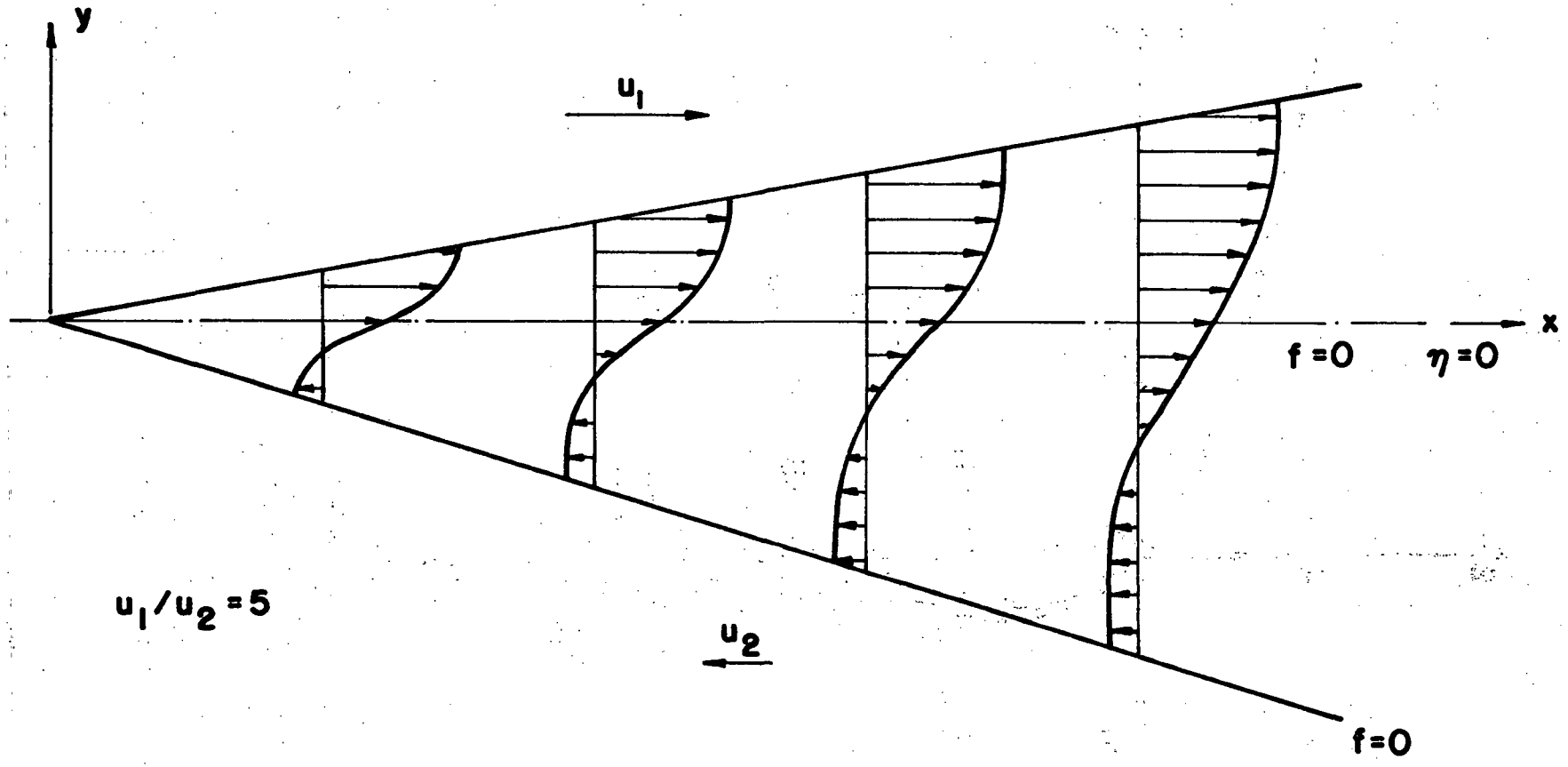

Fig. 34 Similar solution

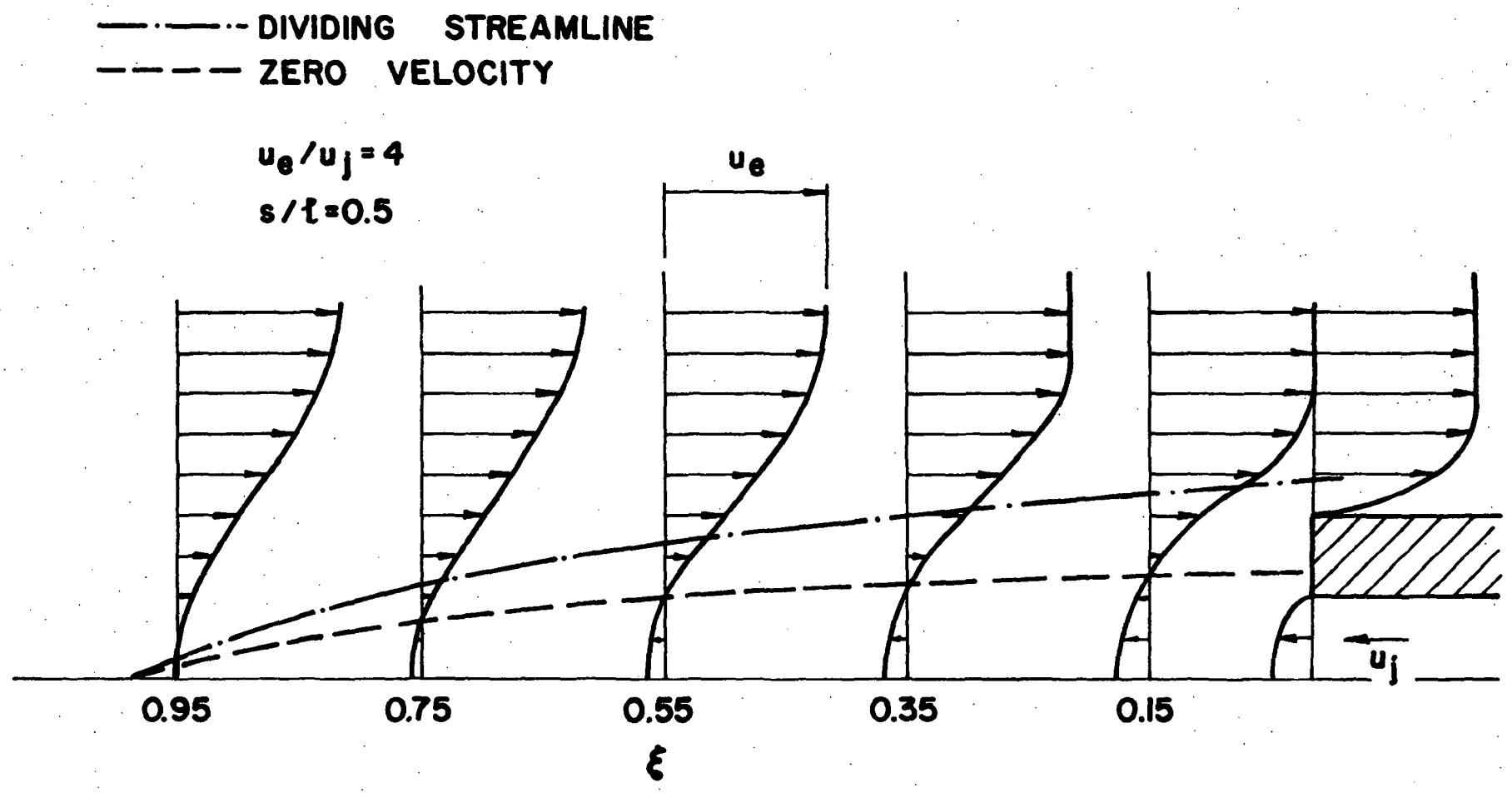

Fig. 35 Non-similar solution; velocity profiles distribution

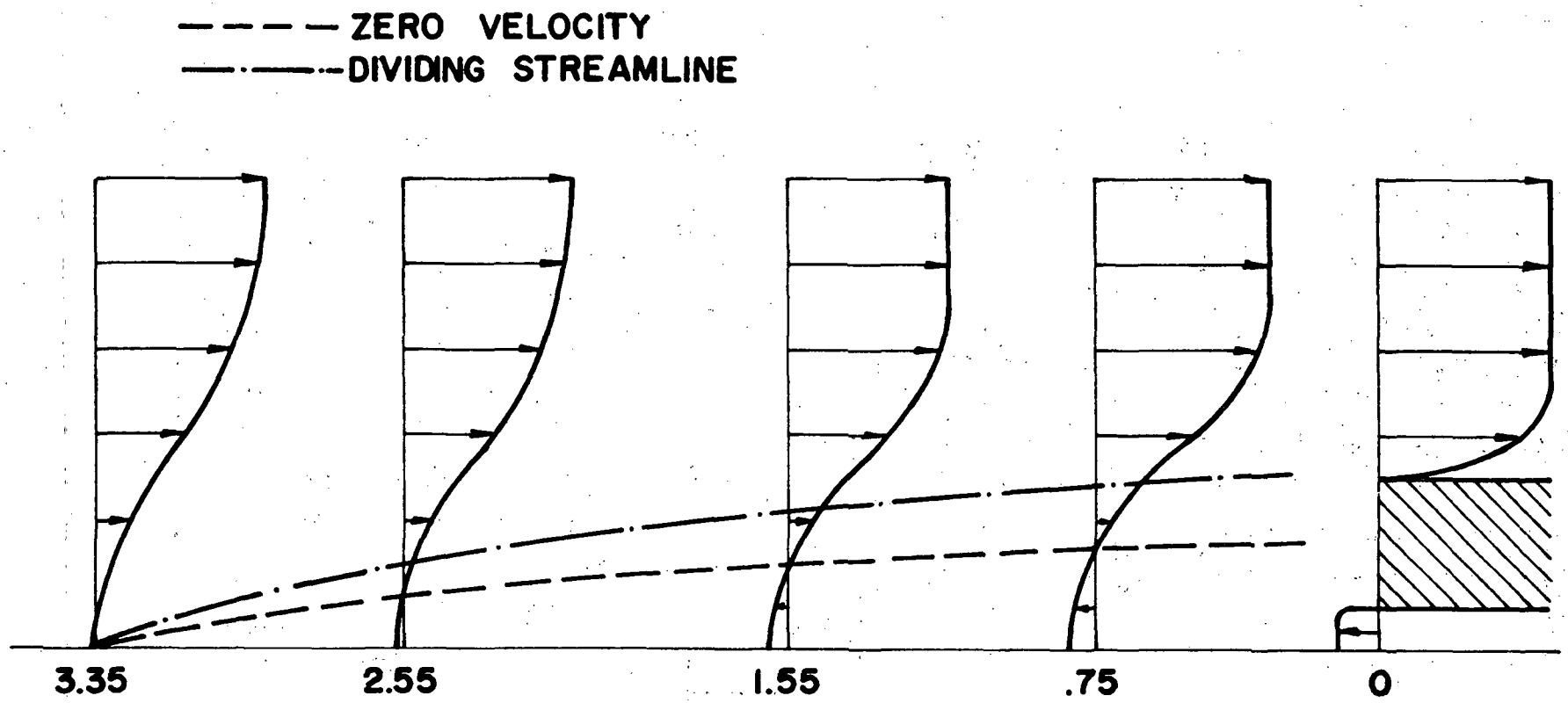

Fig. 36 Non-similar solution; velocity profiles distribution

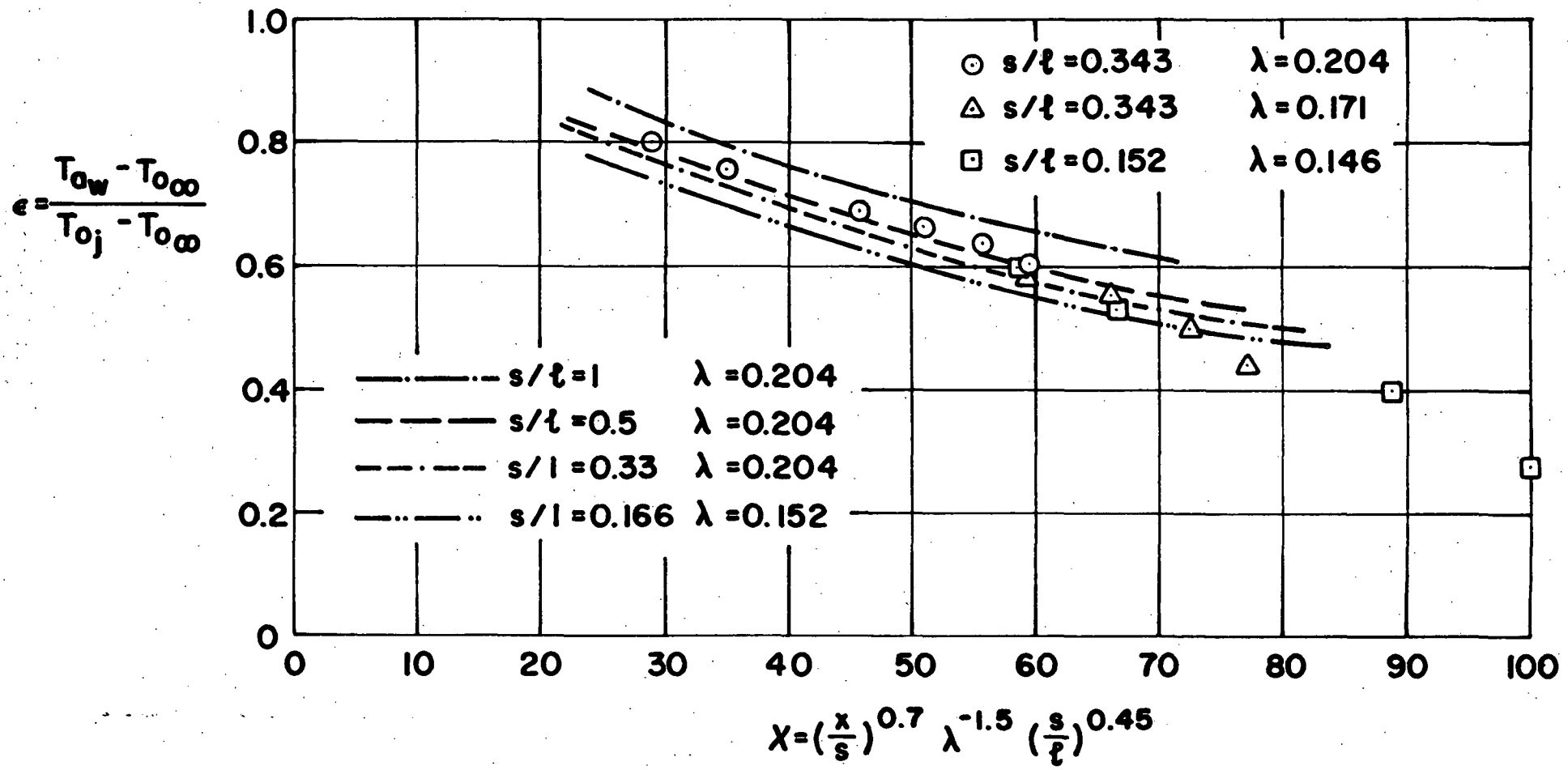

Fig. 37 Cooling effectiveness; experimental and theoretical results

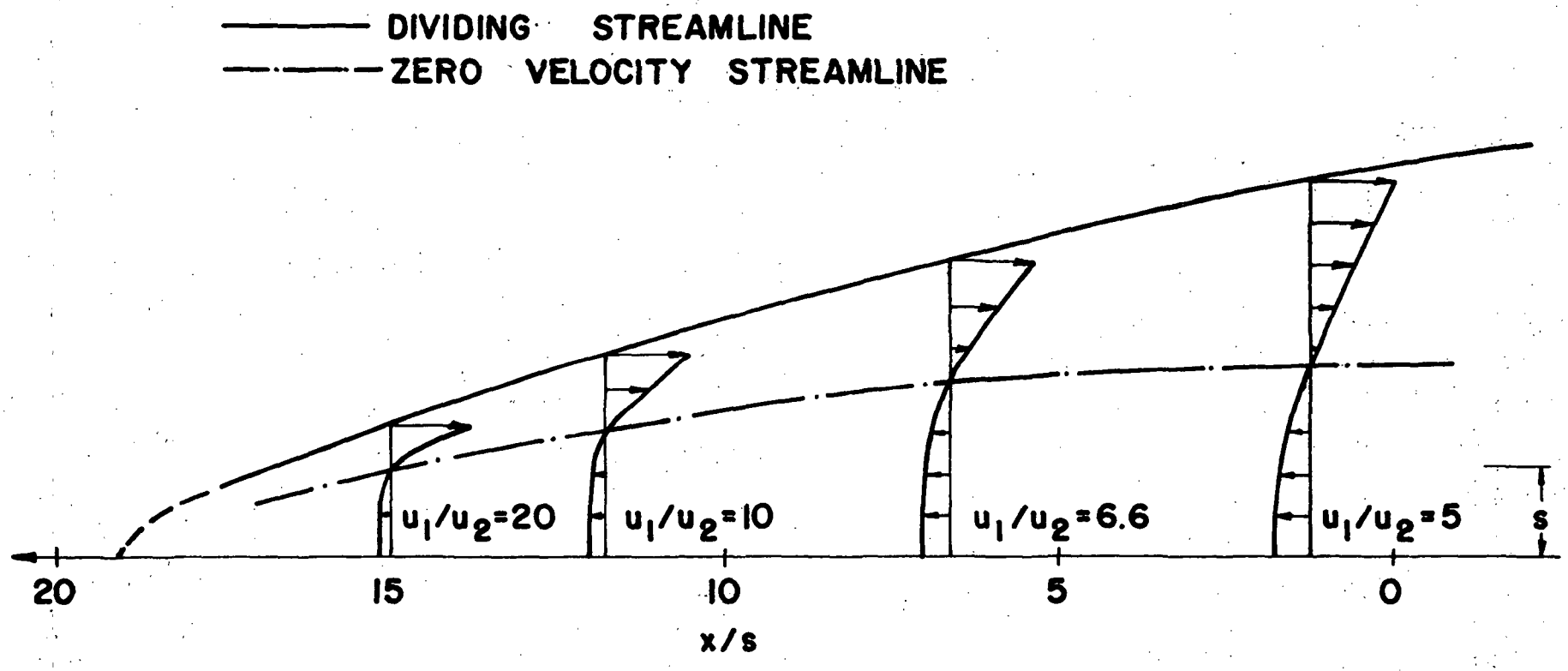

Fig. 38 Locally similar solution; velocity profiles distribution

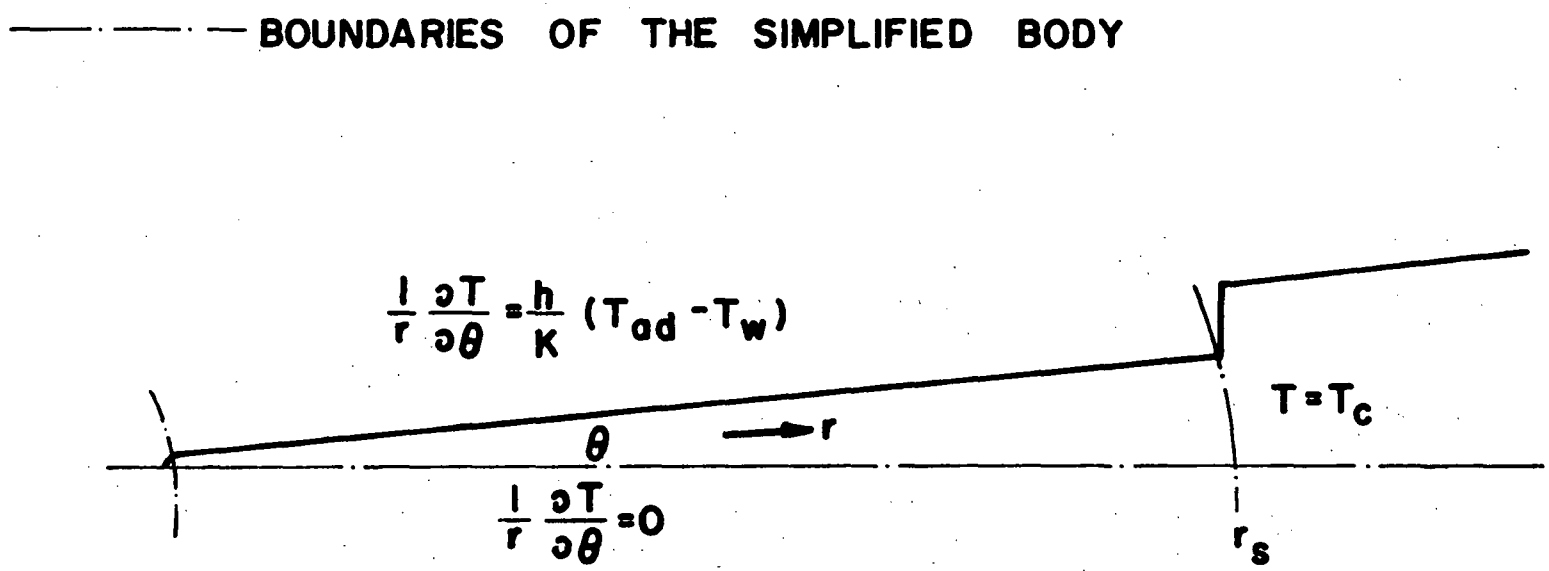

Fig. 39 Geometry and boundary conditions for the internal heat conduction problem

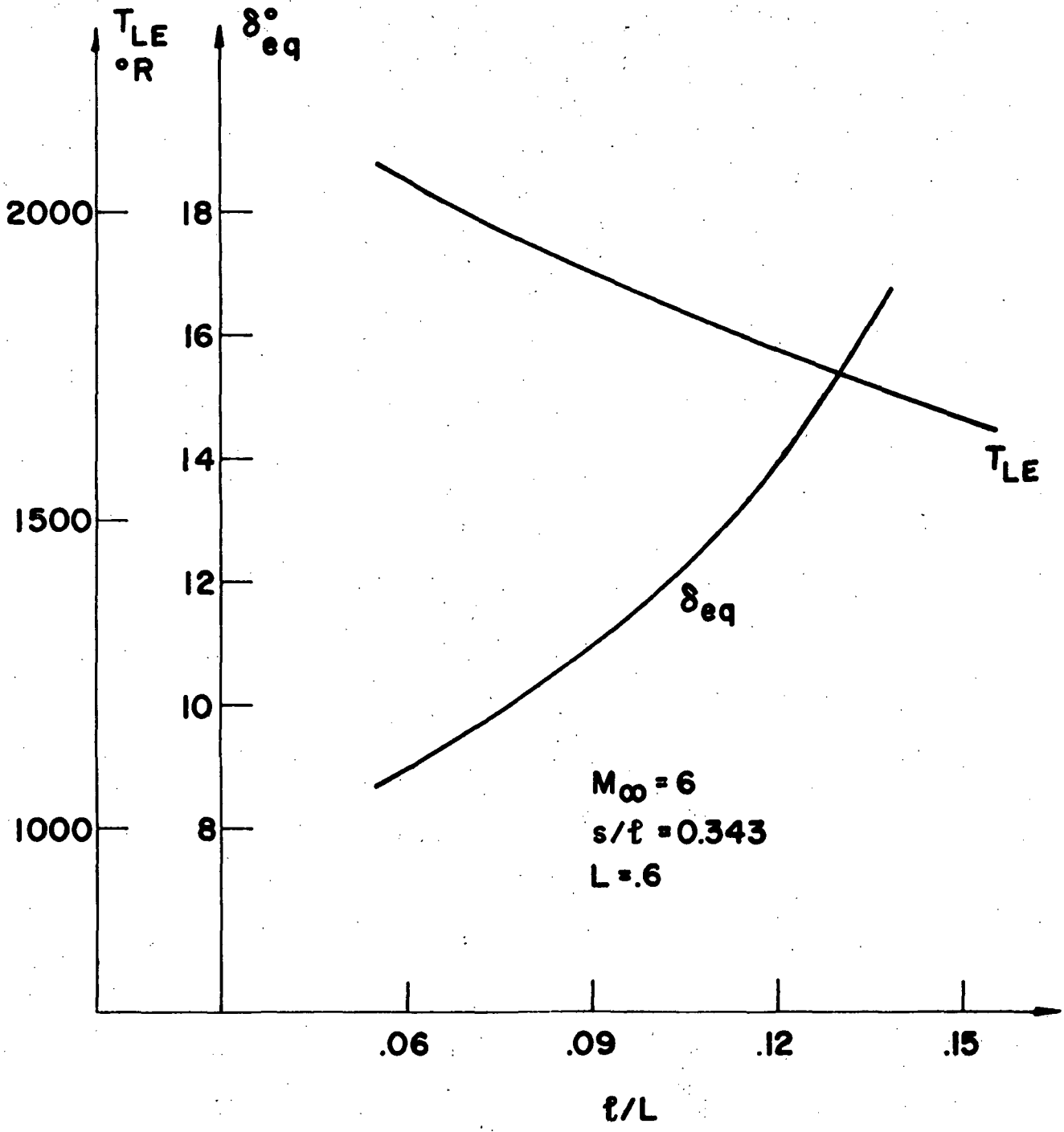

Fig.40 Temperature and equivalent body slope distribution

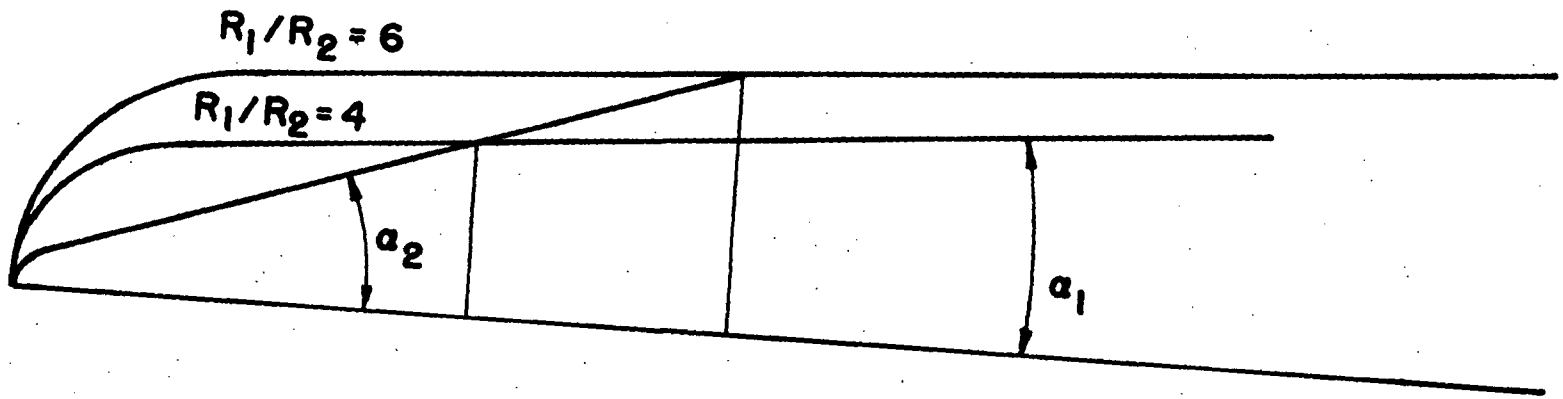

Fig. 41 Body shapes used for comparing total pressure bodies

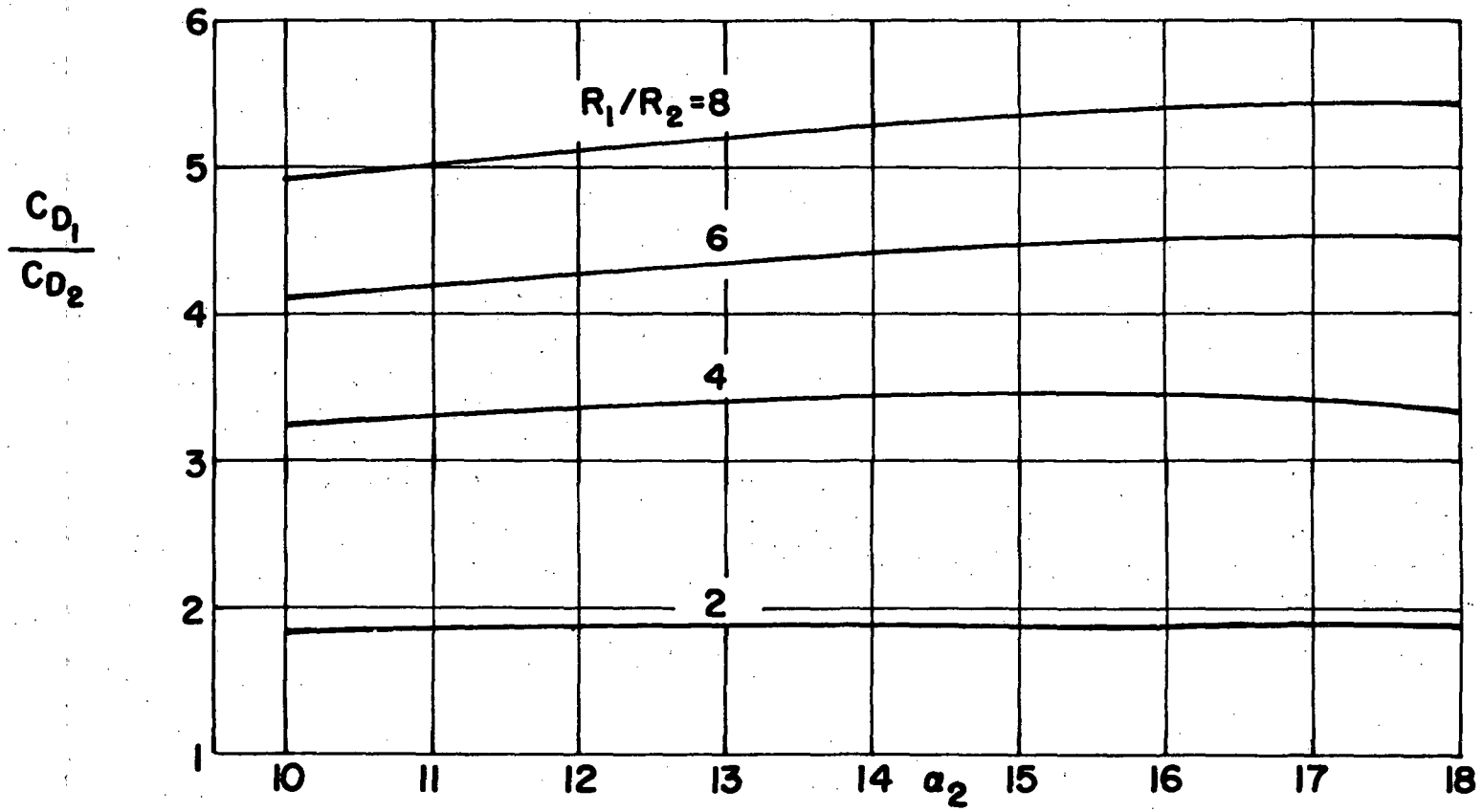

Fig. 42 Drag coefficients ratio of two different cooling streams

APPENDIX I

Quasi-linearization of the System in 5b

To solve numerically the free boundary value problem the following quasi-linearization method was used. Here u is assumed to be

$$u^{\nu+1} = u^{\nu} + \Delta u$$

where superscript ν is the interaction counter and u^{o} is an assumed solution that satisfies the boundary conditions. In the first interaction the position of the boundary is assumed known. In subsequent interactions the free boundary location is shifted if the condition given by Eq. (5) is not satisfied.

The equation (10) becomes linear in Δu

$$a(\Delta u)'' + b(\Delta u)' + c\Delta u + d = 0 \qquad (I,1)$$

with

$$\Delta u(\eta_1) = 0$$

$$\Delta u(\eta_2) = 0$$

In (I,1) a, b, c, d, are functions of B, C, u^{ν}, (u^{ν}), $(u^{\nu})''$ and f which is calculated by

$$f = \int_{o}^{n} u^{\nu}\, d\eta$$

After expressing the derivatives of Δu in finite differences the linear second order equation (I,1) reduces to a tridiagonal system (for the N values of Δu at each η) with boundary conditions specified at each end.

For every value of the boundary, the calculation is repeated until convergence $\left(\frac{\Delta u}{u} < \epsilon\right)$. If this solution does not satisfy the free boundary condition

$$\int_{o}^{n_o} u\, dn = 0$$

the boundary is moved and the calculation repeated until convergence.

APPENDIX II

Non-Similar Solutions for the Velocity and Temperature Profiles

Analytical expressions of the velocity profiles are derived here as solutions of the Eq. (13). The initial condition (15) for the velocity profile are assumed to be:

$$
\begin{aligned}
w(0,y) &= B + cy + gy^2 > 0 && 0 < y < y_j \\
&= 0 && y_j < y < y_s \\
&= d + ay + by^2 < 0 && y_s < y < y_e \\
&= A && y_e < y
\end{aligned}
\qquad (\text{II},1)
$$

where ye = ys+δ and δ is the assumed thickness of the mainstream boundary layer. The coefficients in (I,1) are found imposing the conditions

$$
\begin{array}{llll}
y=0 & u=u_j & y=y_s & u=0 \\
 & \dfrac{\partial u}{\partial y}=0 & y=y_e & u=u_e \\
y=y_j & u=0 & & \dfrac{\partial u}{\partial y}=0
\end{array}
\qquad (\text{II},2)
$$

This initial profile is shown in Fig. 35 and 36 for two different conditions. With the initial condition (II,1) the solution (18), after evaluating the integrals appearing in it, can be expressed in the form:

$$
\begin{aligned}
u(\xi,y) = {} & \left[\frac{B}{2}\left(1-gy^2\right)+gy^2+g\xi\right]\left[\operatorname{erf}\left(\frac{y+y_j}{2\xi^{1/2}}\right)-\operatorname{erf}\left(\frac{y-y_j}{2\xi^{1/2}}\right)\right] + \\
& + \left[\frac{A-d-by^2}{2}-b\xi\right]\left[\operatorname{erf}\left(\frac{y+y_e}{2\xi^{1/2}}\right)-\operatorname{erf}\left(\frac{y-y_e}{2\xi^{1/2}}\right)\right] + \\
& + \frac{ay}{2}\left[\operatorname{erf}\left(\frac{y+y_s}{2\xi^{1/2}}\right)+\operatorname{erf}\left(\frac{y-y_e}{2\xi^{1/2}}\right)\right] + \left[\frac{d+by^2}{2}+b\xi\right]\left[\operatorname{erf}\left(\frac{y+y_j}{2\xi^{1/2}}\right)-\operatorname{erf}\left(\frac{y-y_s}{2\xi^{1/2}}\right)\right] + \\
& + \left[\frac{2\xi^{1/2}}{\sqrt{\pi}}\,g\left(\frac{y+y_j}{2}\right)\right]\left[e^{-\left(\frac{y+y_j}{2\xi^{1/2}}\right)^2}-e^{-\left(\frac{y-y_j}{2\xi^{1/2}}\right)^2}\right] - \frac{ay}{2}\left[\operatorname{erf}\left(\frac{y+y_s}{2\xi^{1/2}}\right)+\operatorname{erf}\left(\frac{y-y_s}{2\xi^{1/2}}\right)\right] + \\
& + \frac{2\xi^{1/2}}{\sqrt{\pi}}\left(\frac{a-2by}{2}\right)\left[e^{-\left(\frac{y+y_e}{2\xi^{1/2}}\right)^2}-e^{-\left(\frac{y+y_s}{2\xi^{1/2}}\right)^2}\right] + \frac{2\xi^{1/2}}{\sqrt{\pi}}\left(\frac{a+2by}{2}\right)\left[e^{-\left(\frac{y-y_e}{2\xi^{1/2}}\right)^2}-e^{-\left(\frac{y-y_s}{2\xi^{1/2}}\right)^2}\right] + \\
& + \frac{b\xi^{1/2}}{\sqrt{\pi}}\left[(y+y_e)e^{-\left(\frac{y+y_e}{2\xi^{1/2}}\right)^2}-(y+y_s)e^{-\left(\frac{y+y_s}{2\xi^{1/2}}\right)^2}-(y-y_e)e^{-\left(\frac{y-y_e}{2\xi^{1/2}}\right)^2}+(y-y_s)e^{-\left(\frac{y-y_s}{2\xi^{1/2}}\right)^2}\right] - A
\end{aligned}
$$

By varying the values of ys, yj, uj, uj', ue, different flow fields can be represented. Two examples are illustrated in Fig. (35) and (36). For the total temperature the initial condition can be expressed in a first approximation with

$$T_o(o,y) = T_{o_j} \quad 0 < y < y_j$$

$$T_{o_B} \quad y_j < y < y_s$$

$$T_{o_e} \quad y_s < y \tag{II,3}$$

where T_{o_b} is the average total temperature of the recirculation region in front of the step. This temperature was computed as a first approximation with a global energy balance and can be expressed by

$$T_{o_B} = \frac{\dfrac{r_e T_{oe} + r_j T_{oj} \lambda}{1+\lambda} + r_j T_{oj} \lambda}{1+\lambda}$$

where r is the recovery factor.

With the initial condition (II,3) the solution is

$$T_o(\xi, y) = \frac{T_{oe}}{2}\left[2 + \operatorname{erf}\left(\frac{y+y_e}{2\xi^{1/2}}\right) - \operatorname{erf}\left(\frac{y-y_e}{2\xi^{1/2}}\right)\right. +$$

$$+ \frac{T_{oB}}{2}\left[\operatorname{erf}\left(\frac{y+y_e}{2\xi^{1/2}}\right) - \operatorname{erf}\left(\frac{y-y_e}{2\xi^{1/2}}\right) - \operatorname{erf}\left(\frac{y+y_j}{2\xi^{1/2}}\right) + \operatorname{erf}\left(\frac{y-y_j}{2\xi^{1/2}}\right)\right] +$$

$$+ \frac{T_{oj}}{2}\left[\operatorname{erf}\left(\frac{y+y_j}{2\xi^{1/2}}\right) - \operatorname{erf}\left(\frac{y-y_j}{2\xi^{1/2}}\right)\right]$$

from which it is possible to obtain the value of the wall and consequently the effectiveness ϵ. The results for different cases are plotted in Fig. 37 and are compared with the experimental results.